Metal-Metal Interactions in Trinuclear Copper(II) Complexes $[Cu_3(R\text{-}COO)_4(H_2TEA)_2]$ and Binuclear $[Cu_2(RCOO)_2(H_2TEA)_2]$. Syntheses and Combined Structural, Magnetic, High-Field EPR and Theoretical Studies.

Andrew Ozarowski[a*], Carmen J. Calzado[b*], Raj Pal Sharma[c], Santosh Kumar[c], Julia Jezierska[d], Celestino Angeli[e] , Federico Spizzo[g], Valeria Ferretti[e,f*]

[a]National High Magnetic Field Laboratory, Florida State University, Tallahassee, Florida 32310 United States
[b]Departamento de Química Física, Universidad de Sevilla. c/ Prof. García González, s/n. 41012- Sevilla. Spain.
[c]Department of Chemistry, Panjab University, Chandigarh-160014, India
[d]Faculty of Chemistry, Wroclaw University, 50-383 Wroclaw , 14 F. Joliot Curie Str., Poland.
[e]Dipartimento di Scienze Chimiche e Farmaceutiche and [f]Centro di Strutturistica Diffrattometrica, Università di Ferrara. Via Fossato di Mortara 17-27, I-44121, Ferrara, Italy.
[g]Dipartimento di Fisica e Scienze della Terra, Università di Ferrara, Via Saragat 1, I-44122 Ferrara, Italy

*** e-mail: ozarowsk@magnet.fsu.edu (AO); calzado@us.es (CJC); frt@unife.it (VF)**

Abstract

The trinuclear $[Cu_3(R\text{-}COO)_4(H_2TEA)_2]$ copper(II) complexes, where $RCOO^-$ = 2-furoate (**1**), 2-methoxybenzoate (**2**) and 3-methoxybenzoate (**3**, **4**), as well as dimeric species $[Cu_2(H_2TEA)_2(RCOO)_2]\cdot 2H_2O$, have been prepared by adding triethanolamine (H_3TEA) at ambient conditions to hydrated $Cu(R\text{-}COO)_2$ salts. The newly synthesized complexes have been characterized by elemental analyses, spectroscopic techniques (IR and UV/Visible), magnetic susceptibility, single crystal X-ray structure determination and theoretical calculations, using a DDCI (Dedicated Difference Configuration Interaction) approach for the evaluation of magnetic coupling constants. In the 2-furoate (**1**) and 2-methoxybenzoate (**2**) the central copper atom lies on an inversion center, while in the two polymorphic forms of 3-methoxybenzoate (**3**,**4**) derivatives the three metal centres are crystallographically independent. The zero-field splitting parameters (zfs) of the trimeric compounds, D and E, were derived from high-field, high-frequency EPR spectra at temperatures ranging from 3 K to 290 K and were used for the interpretation of the magnetic data. It was found that the dominant interaction between the terminal and central Cu sites J_{12} is ferromagnetic in nature in all complexes, even if differences have been found between the symmetrical or *quasi*-symmetrical **1-3** complexes and non-symmetrical complex **4**, while the interaction between the terminal centers J_{23} is negligible.

Keywords: Trinuclear copper(II) complexes; Binuclear copper(II) complexes, Carboxylato bridges; Alkoxo bridges; Crystal structure; EPR; Magnetism; DDCI calculations

1. Introduction

Materials exhibiting magnetic properties with potential technological applications are characterized by a close association of magnetic subunits able to communicate with each other. From a synthetic point of view, the use of simple bridging ligands (e.g., methoxide, hydroxide, alkoxide, oxide, carboxylate) to obtain transition-metal complexes has led to the formation of molecular clusters that in some cases behave as 'single-molecule magnets'[1]. Among the transition metals, copper is a good candidate for assembly of multinuclear clusters due to its variable coordination number and geometry, which can be conjugated with the versatility of the employed ligands. Actually, besides magnetism[2] multinuclear copper(II) complexes have proved to be of considerable interest in many modern research areas such as catalysis[3], DNA cleavage[4], oxygen activation[5] and host-guest equilibria[6] . The choice of the polyfunctional ligands allows a rational approach to obtain predetermined molecular architectures and in this context carboxylates have proved to be very efficient bridging ligands. Copper (II)-carboxylate complexes may be monomeric, dimeric or polymeric because of diverse coordination modes of carboxylate group. Dinuclear triply bridged copper(II) compounds, for example, can exhibit a great diversity of topologies, in which the coordination around the central metal countinuously changes from regular trigonal bipyramid to regular square-based pyramid[7]. It was found that the coordination mode affects the intramolecular magnetic exchange phenomena and consequently the final magnitude of the magnetic coupling constant, switching the magnetic behavior from ferro- to antiferro magnetic; furthermore, such structural property can be fine-tuned by the use of nitrogen containing non-carboxylic ligands. Among them, triethanolamine is in all respects a versatile ligand, that can be found in its neutral form, H_3L, or mono-, H_2L^-, di-, HL^{2-}, or tri-deprotonated, L^{3-}. We have recently shown that *ortho*-, *meta*- and *para*-methoxybenzoate Cu(II) complexes react with triethanolamine to give dimeric complexes of general formula $[Cu_2(H_2TEA)_2(RCOO)_2]\cdot 2H_2O$[8], showing ferromagnetic or antiferromagnetic behavior depending on the structural properties of the alkoxo bridge. That study was a part of our research on complexes of copper(II) arylcarboxylates with nitrogen-donor ligands[9] .

While further exploring the reactions of Cu(II) carboxylates with triethanolamine, we isolated new trinuclear Cu(II) complexes with formula $[Cu_3(R\text{-}COO)_4(H_2TEA)_2]$, where $RCOO^-$ is 2-furoate (**1**), 2-methoxybenzoate (**2**) and 3-methoxybenzoate (**3**, **4**). Thus, in the cases of the *ortho*- and *meta*-methoxybenzoates, we have prepared both the dimeric and trinuclear complexes.

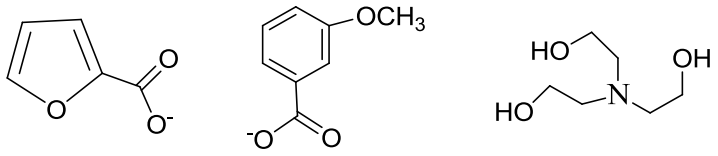

furan-2-carboxylate *m*-methoxybenzoate H_3TEA

Scheme1- Ligands used in this study

Similar binuclear and trinuclear compounds based on hetero triply-bridged di- and trinuclear,[8,10,11,12,13] Cu(II) units with carboxylato and hydroxo (or alkoxo) bridges have been reported previously, most of them presenting ferromagnetic behavior. While the binuclear Cu(II) bis(μ-hydroxo) and bis(μ-alkoxo) show a clear correlation between structure and magnetism (correlation between *J* and the Cu-O-Cu bonding angle and the Cu-OR-Cu torsion angle)[14], the rationalization of the magnetic behavior in systems containing hetero bridges is more difficult and usually based on the concept of the complementarity / countercomplementarity between the ligand and metal orbitals, concept introduced by Nishida et al.[15] and McKee et al.[16] to explain the effect of different bridging ligands on the magnetic coupling.

The present work is aimed at synthesis, characterization of these new copper(II) triethanolamine complexes and studying their magnetic properties by a multifaceted approach combining X-ray structure determination, magnetic susceptibility measurements, high-field, high-frequency EPR spectroscopy and theoretical calculations. The results of these different methodologies provide information about the Heisenberg and zero-field splitting parameters, and insights into the main mechanisms involved in the magnetic coupling interaction inside a complex. To the best of our knowledge, this is the first time that the magnetic properties of trimeric Cu(II) complexes have been explored in fine details using HF EPR spectroscopy. Additionally, the high field EPR spectra of the corresponding dinuclear compounds[8] have been recorded and their description completed.

2. Experimental

2.1 Materials and instruments

Analytical grade reagents were used throughout this work without any further purification. Carbon, Hydrogen and Nitrogen were determined micro-analytically by automatic Perkin Elmer 2400 CHN-elemental analyzer and copper was determined by standard literature methods[17] using the Vario EL III Element Analyzer, (Elementar Analysensysteme GmbH) for C, H, N and (ARL)-Model 3410-ICP Spectrometer for Cu.

FT-IR spectrum of compound **1** was recorded as KBr pellet on PERKIN ELMER SPECTRUM RXFT-IR system (India). Infrared (IR) spectra of compounds **2-4** were recorded over the range 400–4000 cm^{-1}in KBr pellets using Bruker 113v spectrophotometer.

The NIR-Vis-UV diffuse-reflectance electronic spectra of compounds **1 - 4** as well as of the dimeric complexes were recorded on a Cary 500 Scan spectrophotometer with measure step of 10 cm^{-1} in the 5000-50000 cm^{-1} spectral range at room temperature.

2.2 Synthesis

Complex **1,** $[Cu_3(2\text{-furoate})_4(H_2TEA)_2]$. Sodium salt of 2-furoic acid was prepared in situ by dissolving 0.16 g (4 mmol) of NaOH and 0.44 g (4 mmol) of 2-furoic acid in minimum amount of water (Eq.(R1)). 0.50 g (2 mmol) of hydrated copper sulphate, $CuSO_4.5H_2O$ was dissolved in 10 mL of distilled water. On mixing the two solutions, copper(II) furanoate precipitated immediately, as shown by Eq. (R2).

$$HL + NaOH \xrightarrow[R.T.]{H_2O} NaL + H_2O \qquad (R1)$$

where HL= furan-2-caboxylic acid

$$CuSO_4.5H_2O + 2NaL \xrightarrow[R.T.]{H_2O} Cu(L)_2.nH_2O \qquad (R2)$$

The precipitated product was filtered, washed with water followed by methanol and dried at room temperature (yield 85%). Triethanolamine was added dropwise to the suspension of copper(II) furoate in 20 mL of a methanol-water mixture (4:1 v/v). The addition was continued till a clear greenish blue colored solution was obtained. When the solution was allowed to evaporate slowly at room temperature, blue colored shiny crystals appeared after few days, in accordance with Eq. (R3), which were separated from the mother liquor and dried in air.

Other three trinuclear complexes, **2**, **3** and **4** were prepared in a procedure in which previously reported analogous dimeric complexes were obtained.[8] In the case of the ortho- and meta- methoxybenzoates, first the trinuclear species precipitated from the mother liquor and subsequently, in some preparations the dimeric complexes crystallized in the filtrate. Very pure samples of either dimeric or trinuclear species could be obtained. Raw **2** was recrystallized from MeCN, while **3** and **4** were obtained by recrystallization of the corresponding crude product from methanolic solutions. **3** can also be prepared by recrystallization of **4** from hot methanol, but no good crystals could be obtained in this way. The unpredictability of the synthesis and formation of both tri- and binuclear complexes in the same reaction mixture was also reported by others.[12b,13] It seems that the formation of either dinuclear or trinuclear products is determined by the conditions in the solution when the crystallization starts and the outcome is difficult to control. Once a dimeric species has been formed, it is not possible to recrystallize it into a trinuclear species, and no opposite process occurs. Possibility of the EPR identification of the products and purity assessment immediately after the synthesis was a big advantage in this work. No trinuclear paramethoxybenzoate and no pure dimeric furanoate could be obtained. It is thus clear that the reaction may occur in two ways.

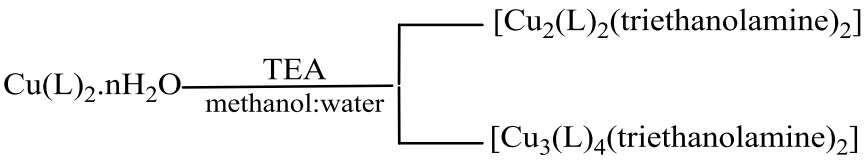

(R3)

Interestingly, in all cases in which the trinuclear complexes were obtained in this paper, the raw intermediate carboxylate species were proven by EPR to be high-purity dimeric "paddlewheel" complexes $[CuL_2]_2(H_2O)_2$, similar to copper acetate monohydrate and showing typical EPR parameters (Table S3, Figs S6-S7). In the p-methoxybenzoic acid system, where only a dimer $[Cu_2(H_2TEA)_2(RCOO)_2]\cdot 2H_2O$ was obtained, the intermediate was a mixture of two slightly different monomeric species (Fig S7).

All complexes are soluble in methanol and in acetonitrile, but insoluble in water.

Complex **1,** $[Cu_3(2\text{-furoate})_4(H_2TEA)_2]$ decomposes at 185°C. FT IR (KBr) (ν_{max}, cm^{-1}): 3140(w), 2966(w), 2881(w), 1599(s), 1561(m), 1416(m), 1365(s), 1224(s), 1197(m), 1137(m), 1087(m), 1006(s), 901(m), 779(s), 621(s), 526(w), 487(s). Anal. calcd. for

$C_{32}H_{40}Cu_3N_2O_{18}$ (%): C, 41.24; H, 4.29; N, 3.00; Cu, 20.46; Found: C, 41.05; H, 4.58; N, 2.92.1; Cu, 20.12.

Complex **2,** [Cu_3(*o*-methoxybenzoato)$_4$(H_2TEA)$_2$]·2(C_2H_3N). FT IR (KBr) (ν_{max}, cm^{-1}): 3388(m, broad), 2929(m), 2881(m), 1602(s), 1564(s), 1409(s), 1382(s), 1250(s), 1084(m), 1026(m), 897(m), 831(w), 756(m). Anal calcd. for $C_{48}H_{62}O_{18}N_4Cu_3$: (%) C 49.12, H5.32, N 4.77, Cu 16.24. Found: C 49.0. H 5.4, N 4.80, Cu 16.15.

Complex **3,** [Cu_3(*m*-methoxybenzoato)$_4$(H_2TEA)$_2$]. FT IR (KBr) (ν_{max}, cm^{-1}): 3223(m, broad), 2929(m), 1558(s), 1450(s), 1392(s), 1252(s), 1093(m), 1037(s), 908(m), 762(s). Anal. Calcd for $C_{44}H_{56}O_{18}N_2Cu_3$: (%) C 48.41, H5.17, N 2.57, Cu 17.46. Found: C 48.3, H 5.22, N 2.49, Cu 17.55.

Complex **4,** [Cu_3(*m*-methoxybenzoato)$_4$(H_2TEA)$_2$]. FT IR (KBr) (ν_{max}, cm^{-1}): 3409(m, broad), 2941(m), 1603(m), 1554(s), 1452(m), 1390(s), 1248(m), 1286(w), 1083(m), 1045(m), 906(w), 773(m). Anal. Calcd. same as **3**. Found (%) C 48.2, H 5.0, N 2.47, Cu 17.40

2.3 X-ray crystallography

Single-crystal diffraction data for **1-4** were collected on a Nonius Kappa diffractometer equipped with a CCD detector with graphite-monochromatized MoKα radiation (λ = 0.71069 Å). Intensities were corrected for Lorentz, polarization and absorption[18] effects. The structures were solved by direct methods with the SIR97 suite of programs[19] and refinement were performed on F^2 by full-matrix least-squares methods with all non-hydrogen atoms anisotropic. Hydrogen atoms of TEA ligands in **1** and of OH type in **2-4** were found in the difference Fourier map and refined isotropically; all other hydrogens were included on calculated positions, riding on their carrier atoms. All calculations were performed using SHELXL-97[20] implemented in the WINGX[21] system of programs

2.4 EPR and magnetic susceptibility

Magnetic susceptibility measurements over the temperature range 1.8-300 K were performed at a magnetic field of 0.5 T using a Quantum Design SQUID MPMSXL-5 magnetometer. Correction for the sample holder, as well as the diamagnetic correction χ_D, which was estimated from the Pascal constants,[22] was applied.

High-field, high-frequency EPR spectra at temperatures ranging from ca. 3 K to 290 K were recorded on a home-built spectrometer at the EMR facility of the NHMFL[23] with the microwave frequencies 52-416 GHz. The instrument is a transmission-type device and uses

no resonance cavity. The microwaves were generated by a phase-locked Virginia Diodes source, generating frequency of 13 ± 1 GHz, and equipped with a cascade of frequency multipliers to generate higher harmonic frequencies. A superconducting magnet (Oxford Instruments) capable of reaching a field of 17 T was employed. Additionally, X-band and Q-Band spectra were recorded on a Bruker ElexSys E500 instrument equipped with an NMR teslameter ER 036TM and a frequency counter E 41 FC (Faculty of Chemistry, Wroclaw University).

3. Results and Discussion

3.1. X-ray diffraction

The ORTEPIII[24] views of complexes **1-4** and coordination polyhedra around each Cu atom are shown in Figs 1-4, respectively. Experimental details are given in Table 1 and the geometrical parameters for the most important interactions are reported in Table 2.

Figure 1. ORTEP view and atom numbering scheme for [Cu_3(furan-2-carboxylato)$_4$ (H_2TEA)$_2$] (**1**) Thermal ellipsoids are drawn at the 40% probability level**.** Hydrogen bonds are drawn as dashed lines. C-H hydrogen atoms are not shown for clarity. Central and terminal Cu coordination polyhedra are also shown.

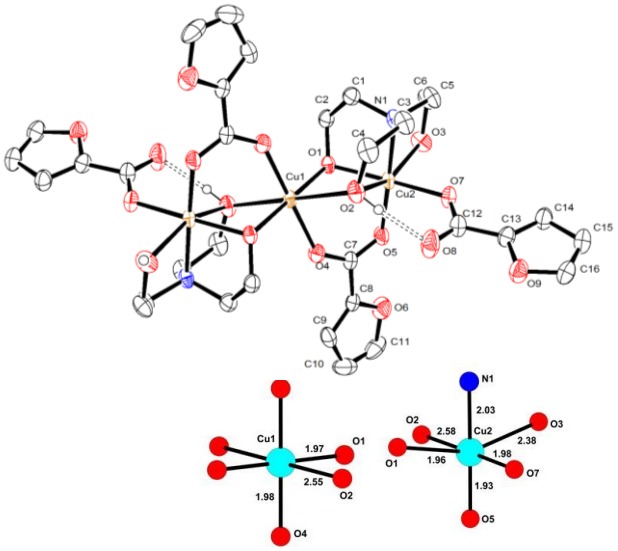

Figure 2. ORTEP view and atom numbering scheme for [Cu_3(*o*-methoxybenzoato)$_4$ (H_2TEA)$_2$]·2(C_2H_3N) (**2**). Thermal ellipsoids are drawn at the 40% probability level**.** Hydrogen bonds are drawn as dashed lines. The solvent molecule and C-H hydrogen atoms are not shown for clarity. Central and terminal Cu coordination polyhedra are also shown.

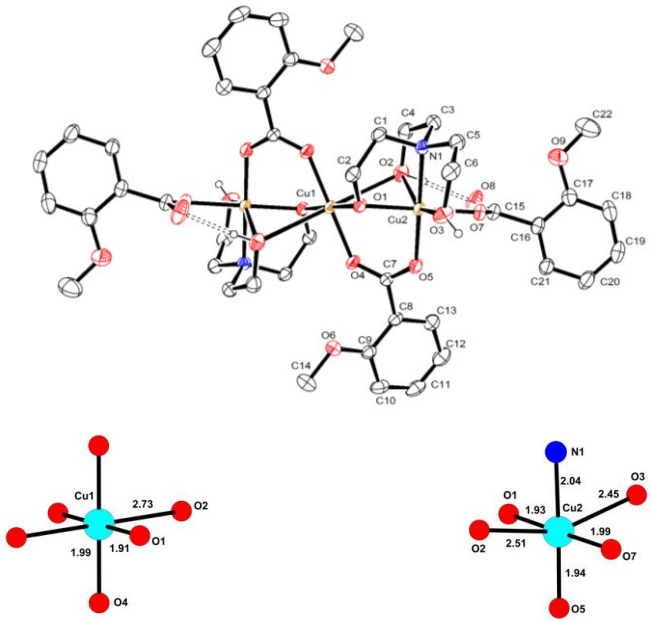

Figure 3. ORTEP view and atom numbering scheme for the approximately centrosymmetric complex [Cu_3(*m*-methoxybenzoato)$_4$(H_2TEA)$_2$] (**3**). Thermal ellipsoids are drawn at the 40% probability level**.** Hydrogen bonds are drawn as dashed lines. C-H hydrogen atoms are not shown for clarity. Central and terminal Cu coordination polyhedra are also shown.

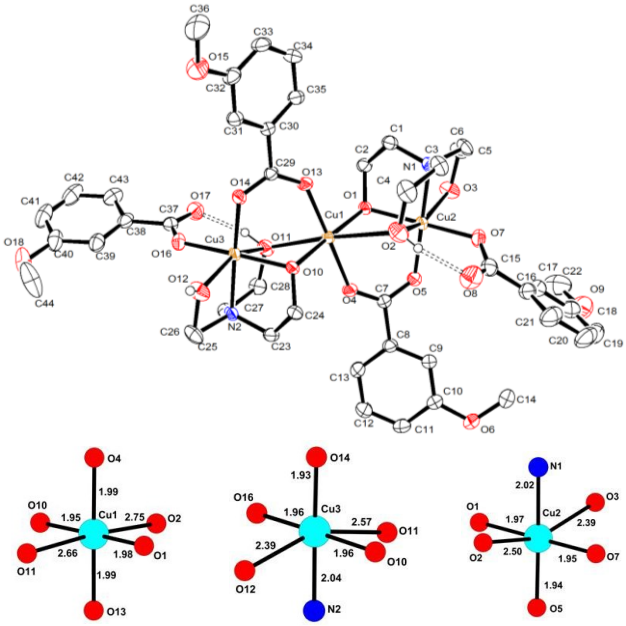

Figure 4. ORTEP views and view and atom numbering scheme for the asymmetric complex [Cu_3(*m*-methoxybenzoato)$_4$(H_2TEA)$_2$] (**4**). Thermal ellipsoids are drawn at the 40% probability level**.** Hydrogen bonds are drawn as dashed lines. C-H hydrogen atoms are not shown for clarity. Central and terminal Cu coordination polyhedra are also shown.

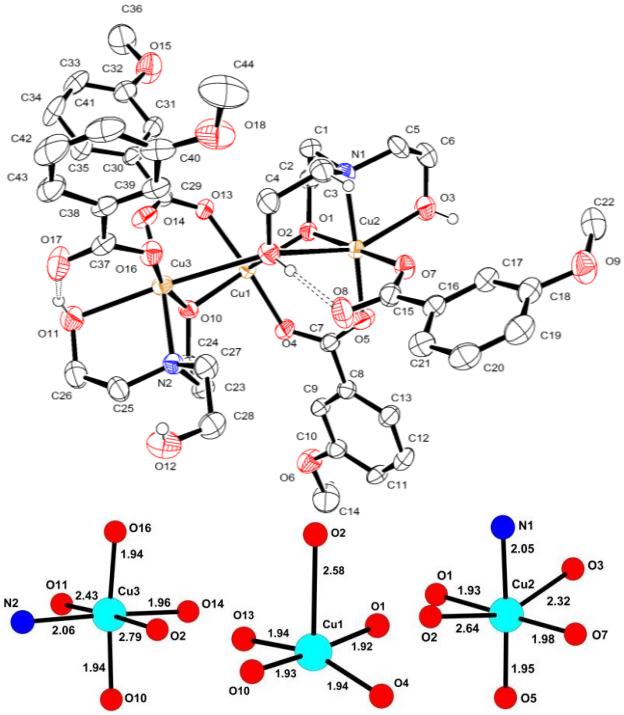

The four polynuclear complexes consist of discrete neutral trinuclear [Cu_3(furan-2-carboxylato)$_4$(H_2TEA)$_2$] (**1**), [Cu_3(*o*-methoxybenzoato)$_4$(H_2TEA)$_2$] (**2**) or [Cu_3(*m*-methoxybenzoato)$_4$(H_2TEA)$_2$] (**3, 4**) species; in **2,** the asymmetric unit is completed by an acetonitrile molecule. In all compounds each copper atom is hetero triply-bridged to the adjacent Cu center by one carboxylato group (*syn-syn* bridging mode), one alkoxo and one OH groups arising from the deprotonated TEA. In **1** and **2** the central Cu1 atom, situated on the inversion center, is bound in an elongated octahedral geometry to six oxygens, two from the furanoic (or benzoic) moiety, and four from the TEA ligand. The mean Cu-O basal distance is 1.96(3) Å, while the protonated O2 oxygens are located in apical positions at a longer distance of 2.554(2) and 2.732(2) Å in **1** and **2**, respectively. The terminal symmetry-related copper atoms are hexacoordinated by a nitrogen and three oxygen atoms from the TEA ligand (two of them protonated, only one deprotonated), an oxygen atom from the carboxylato bridge, and an oxygen from the terminal furan-2-carboxylato or *o*-methoxy-benzoic groups, the apical positions being occupied by O2 and O3 atoms of the TEA ligands (Figures 1 and 2) with Cu-O distances ranging from 2.378(2) Å to 2.580(2) Å. The distance between the adjacent copper(II) ions, as well as the Cu2…Cu2' contact distances, are very similar for the two complexes, being 3.1385(3), 6.2770(4) Å and 3.1201(2), 6.2402(3) Å, for **1** and **2**, respectively. Complexes **3** and **4** are polymorphic forms of the same [Cu_3(*m*-methoxy-carboxylato)$_4$(H_2TEA)$_2$] complex. At variance with the first two structures, the three Cu atoms are crystallographically independent; nevertheless, complex **3** is very similar to **1** and **2**, as far as both the structural parameters and copper atoms coordination are concerned, as it is clearly shown by comparing the geometry of the coordination polyhedra (Figure 3). Conversely, complex **4** shows some peculiarities. While its two lateral copper atoms are hexacoordinated in a similar way as the other compounds, the central Cu1 metal is pentacoordinated to two carboxylate, two alkoxo bridging oxygen atoms and to the O2 protonated oxygen of the TEA ligand in apical position. Actually, the O2-H group in this molecule is triply bound to all three copper atoms. This leads to a second marked difference: while in **1-3** the three metal atoms are arranged in a 'linear' way, forming a Cu2-Cu1-Cu3 angle of 180° (**1** and **2**) or very close to 180° (177.82(2)° in **3**), in **4** this angle is narrowed down to 112.35(1) degrees, bringing Cu2 nearer to Cu3 by more than 1 Å with respect to the linear complexes **1-3**. A list of all relevant bond distances and angles is reported in Table S1 of Supporting Information (SI). Bent trinuclear complexes, similar to **4** have been described, like [$Cu_3(C_6H_5CO_2)_4\{(C_2H_5)_2NC_2H_4O\}_2H_2O$].[10f] However, in those complexes, an oxygen atom of a water molecule bridges all three copper atoms, while in **4** an alkoxo oxygen, a part

of the TEA ligand plays such a role. Increased flexibility of the aquo-bridged complexes compared to **4** results in higher molecular symmetry with a twofold axis passing through the central copper atom.

The TEA/carboxylate trimeric complexes of known structure are compared in Table 3. In all of them the central Cu atom is in a special position, and the 'linear' geometry of **1**-**3**, as well as the octahedral coordination around the three Cu atoms appear to be conserved irrespective of the nature of the carboxylic acid or the possible cocrystallized solvent molecules. In particular, complex **1** is isostructural with TEA/thiophenecarboxylate derivative (AWEQEZ in Table 3, ref. 12a), and shares with it not only the overall geometry but also the packing pattern. Moreover, it is interesting to note that for complexes **2, 3**-**4** the related dimeric forms exist[8] where the carboxylate group is not bridging two different Cu atoms but only one carboxylate oxygen is linked to the central metal. In those dimeric systems, the coordination around the Cu atoms is different in *o*- and *p*-methoxybenzoate complexes, *i.e*. square pyramidal and octahedral respectively, because in the first case the TEA molecule acts as a bidentate ligand instead of tridentate. Such a geometry difference results in a change of the magnetic behavior from antiferro- (o-methoxy) to ferromagnetic (p-methoxy and m-methoxy) in those dimeric compounds.8

Packing. Due to the lack of good hydrogen bonding donors, in all structures only one intramolecular and one intermolecular O-H…O hydrogen bonds are formed (Table 2). In **2**, the cocrystallized solvent molecules are not involved in any strong interaction but simply fill the voids causing consequently the crystal density increase (Table 1). The intramolecular interactions involve the bridging OH of the TEA ligand and the free carboxylate oxygen; the O…O distances vary within the narrow range of 2.609(3)-2.694(4) Å. In complexes **1**-**3**, the intermolecular O-H…O bonds link two adjacent complexes giving for symmetry R2,2(8) ring motifs which in turn are inserted in a C2,2(12) chain. As an example, in Fig. 5 the packing arrangement of **1** is shown; it is characterized by the formation of parallel ribbons running parallel to the *a* axis. Conversely, in **4**, the molecule implies only O7 and O3-H in the R2,2(8) ring motif with the adjacent complex on one side (green hydrogen bonds in Figure 6), while on the opposite side the free O12-H group links the O10 atom of the nearby molecule giving rise to a C1,1(7) chain motif (red hydrogen bonds in Figure 6). The resulting ribbons are not parallel to a crystallographic direction but bisect the a,b plane. In all structures, a number of weak C-H…O interactions contribute to the crystal robustness (Table S2 in SI), while no π…π interactions between the aromatic rings were found.

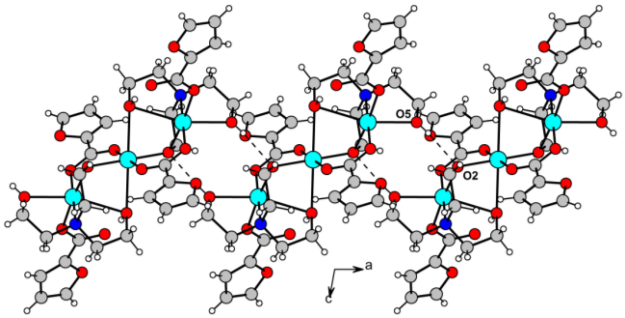

Figure 5. Packing pattern of complex **1.** Intermolecular hydrogen bonds are drawn as broken lines

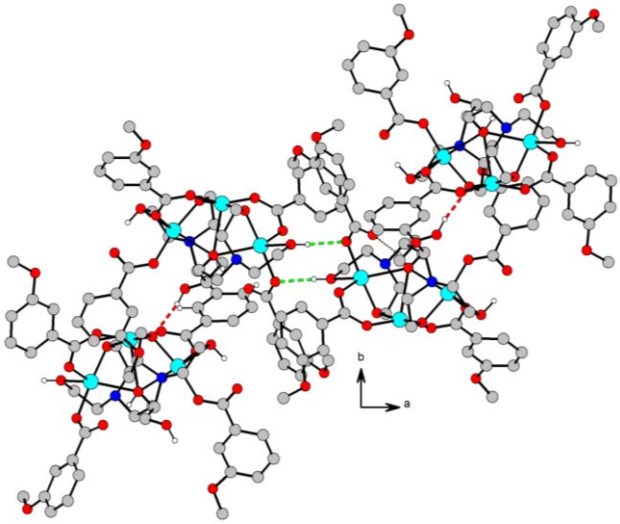

Figure 6. Packing pattern of complex **4.** Intermolecular hydrogen bonds are drawn as broken lines (see text). For the sake of clarity, hydrogen atoms bound to carbon atoms are not shown.

Table 1. Crystal data for trimeric copper(II) complexes

	1	**2**	**3**	**4**
Chemical formula	$C_{32}H_{40}Cu_3N_2O_{18}$	$C_{44}H_{56}Cu_3N_2O_{18}$. $2(C_2H_3N)$	C_{44} $H_{56}Cu_3N_2O_{18}$	C_{44} $H_{56}Cu_3N_2O_{18}$
M_r	931.28	1173.67	1091.56	1091.56
Space Group	Triclinic, P-1	Monoclinic, $P2_1/c$	Triclinic, P-1	Monoclinic, $P2_1/c$
Z	1	2	2	4
a, b, c (Å)	8.5790 (2), 9.4128 (2), 11.6658 (3)	11.6469(2), 15.8467(3), 14.0542(3)	8.44460(10), 16.8601(2), 16.9374(3)	13.4231(1), 13.4250(1) 26.0803(3)
α, β, γ (º)	97.114 (1), 99.975 (1), 92.867 (1)	90, 93.566(1), 90	89.0670(6), 81.1580(7) 82.6680(6)	90, 98.1420(4), 90
V (Å^3)	918.19 (4)	2588.89(9)	2363.34(6)	4652.43(7)
D_c/g cm^{-3}	1.684	1.506	1.534	1.558
μ (mm^{-1})	1.80	1.30	1.41	1.44
Crystal size (mm)	0.35 × 0.23 × 0.17	0.55 x 0.29 x 0.20	0.20 x 0.15 x 0.09	0.47 x 0.12 x 0.10
No. of measured, independent and observed [$I > 2\sigma(I)$] reflections	13956, 4435, 3521	19508, 7547, 5642	25241, 11356, 8336	40773, 11114, 8061
R_{int}	0.045	0.049	0.036	0.062
$R[F^2 > 2\sigma(F^2)]$, $wR(F^2)$, S	0.036, 0.108, 1.06	0.044, 0.130, 1.07	0.047, 0.119, 1.09	0.041, 0.102, 1.06
No. of reflections	4435	7547	11356	11114
No. of parameters	318	335	620	620
$\Delta\rho_{max}$, $\Delta\rho_{min}$ (e Å^{-3})	1.07, −0.76	0.40, -1.08	0.70, -0.70	0.71, -0.87

Table 2. Structural parameters (Å , °) for hydrogen bonds

D-H	D...A	H...A	D-H.....A	
1				
O2-H...O8	0.84(3)	2.665(4)	1.83(3)	172(3)
O3-H...O1^{i}	0.74(4)	2.818(2)	2.07(4)	174(5)
Equivalent positions: (i) 2-x,1-y,-z				
2				
O2-H...O8	0.84(3)	2.660(3)	1.84(3)	162(3)
O3-H...O7^{i}	0.86	2.918(2)	2.09	161
Equivalent positions: (i) -x-1,-y,-z;				
3				
O2-H….O8	0.80(5)	2.693(4)	1.92(5)	163(4)
O11-H...O17	0.87(3)	2.650(4)	1.80(3)	166(2)
O3-H...O10^{i}	0.85(3)	2.768(3)	1.97(3)	155(3)
O12-H...O1^{ii}	0.84(3)	2.754(3)	1.99(4)	150(3)
Equivalent positions: (i) x+1,y,z; (ii) x-1,y,z				
4				
O2-H...O8	0.87(3)	2.609(3)	1.77(3)	164(3)
O11-H...O17	0.89(4)	2.637(3)	1.77(4)	163(4)
O3-H...O7^{i}	0.84(2)	2.864(3)	2.05(2)	164(2)
O12-H...O10^{ii}	0.84(6)	2.908(3)	2.07(6)	170(5)
Equivalent positions: (i) 2-x,-y,2-z; (ii) 1-x,y-1/2,3/2-z				

Table 3. Geometrical parameters of the Cu-O-Cu bridge and fitted J_{12} values of TEA-Cu(II) trinuclear complexes.

CSD code	J_{12} /cm $^{-1}$	Cu-O-Cu angle	carboxylate ligand	Ref.
AWEQEZ	66	75.92 /105.17	thiophene carboxylate	12
AWEQID	66	73.91 / 108.40 73.05 / 107.76	thiophenyl acetate	12
AWEQUP	66	75.69 / 103.69	thiophenyl acetate (solvate)	12
FISJIB	84	76.37 / 104.33	Acetate	11
MEDHUZ	65	73.25 / 109.27	acetate (solvate)	13
MEDJAH	88.9	76.02 / 105.25	formate (solvate)	13
MEDJEL	70.8	77.23 / 105.89	Trifluoroacetate	13
1	77.1	75.37/106.05	furan-2-carboxylate	This work
2	66.4	72.92/108.43	*o*-methoxy-benzoate	This work
3	59.5	73.76/106.46 74.03/107.61	*m*-methoxy-benzoate	This work
4	51.0	71.32/108.05 70.95/104.06	*m*-methoxy-benzoate	This work

3.2. FT-IR Spectroscopy

The infrared spectra of newly synthesized complex salts have been recorded in the region 400-4000 cm^{-1} and tentative bands assignments have been made on the basis of earlier literature reports[25] .

The spectra of the four compounds, shown in Fig. S9 of SI, are very similar. The broad bands in 3140-3409 cm^{-1} region were ascribed to ν(O-H) of triethanolamine. The band at 3140 cm^{-1} in complex **1** appears to be considerably shifted to lower frequency, possibly due to the involvement of O-H groups in strong hydrogen bonding. The absorption bands around 2900-2800 cm^{-1} were assigned to asymmetric and symmetric C-H stretch of furoic/benzoic acids. The bands in the region 1603-1599 cm^{-1} were attributed to ν(C=C) of the furanoic/benzoate moiety. The splitting of bands of $\nu_{as}(COO^-)$ and $\nu_s(COO^-)$ indicated the presence of two types of arylcarboxylate ligands. The bands at 1599/1365 cm^{-1} in **1**, 1562/1382 cm^{-1} in **2,** 1558/1392 cm^{-1} in **3** and 1554/1390 cm^{-1} in **4** were assigned to $\nu_{as}(COO)$, $\nu_s(COO)$ respectively. The $\Delta\nu=\nu_{as}(COO^-) - \nu_s(COO^-)$ separation of 234, 180, 166 and 164 cm^{-1} in **1-4,** respectively, indicates the presence of bidentate or bidentate bridging coordination mode of arylcarboxylate, which was finally confirmed by single crystal X-ray structure determination. The strong to medium bands in the region 1250-1000 cm^{-1} may be attributed to C-N, C-O strech of the triethanolamine ligand.[26] Finally, the IR bands in the 500-400 cm^{-1} region are due to the M-O and M-N stretching vibrations.

3.3. Magnetic susceptibility and HF EPR spectra

Dimeric complexes. The magnetic susceptibility data of dimeric complexes $[Cu_2(H_2TEA)_2(RCOO)_2]\cdot 2H_2O$ derived from the ortho-, meta- and paramethoxybenzoic acid have been reported previously.[8] The copper ion environment in these dimeric complexes is similar to the environment of the terminal copper ions in the trinuclear systems which are the main subject of the present work. Their high-field EPR spectra were therefore recorded (Fig. 7) to help in interpretation of spectra of the trinuclear complexes. The *m*-methoxy and *p*-methoxy dimers are ferromagnetic with the exchange integrals of 101 cm^{-1}, while the *o*-OCH_3 dimer is

antiferromagnetic with J = -83 cm^{-1}. These data refer to the Heisenberg-Dirac-VanVleck Hamiltonian in a form:

$$\hat{\boldsymbol{H}} = -J\,\hat{\boldsymbol{S}}_1 \bullet \hat{\boldsymbol{S}}_2 \qquad (1)$$

The differences in magnetic behavior were discussed in ref 8. The EPR spectra were interpreted in terms of the standard spin Hamiltonian expressed in the total spin S=1 of the system:

$$\hat{\boldsymbol{H}} = \mu_B B\{\mathbf{g}\}\hat{\boldsymbol{S}} + D\{\hat{\boldsymbol{S}}_z^2 - S(S+1)/3\} + E(\hat{\boldsymbol{S}}_x^2 - \hat{\boldsymbol{S}}_y^2) \qquad (2)$$

Instead of using Hamiltonian (2), which is often referred to as the "giant spin Hamiltonian", one can use the spin operators of separate ions.

$$\hat{\boldsymbol{H}} = \mu_B B\{\mathbf{g}_1\}\hat{\boldsymbol{S}}_1 + \mu_B B\{\mathbf{g}_2\}\hat{\boldsymbol{S}}_2 + D_{12}\{\hat{\boldsymbol{S}}_{1z}\,\hat{\boldsymbol{S}}_{2z} - \hat{\boldsymbol{S}}_1\,\hat{\boldsymbol{S}}_2/3\} + E_{12}(\hat{\boldsymbol{S}}_{1x}\,\hat{\boldsymbol{S}}_{2x} - \hat{\boldsymbol{S}}_{1y}\,\hat{\boldsymbol{S}}_{2y}) \qquad (3)$$

The relations between the parameters of these two spin Hamiltonians are (for dimers of S=1/2 ions only):[27]

$$D_{12} = 2\,D, \quad E_{12} = 2\,E \qquad (4)$$

It will be shown in the following text that the {**g**} matrices in the dinuclear and trinuclear systems studied here were found to be non-coaxial with the zero-field splitting tensors. While the tensor quantities had to be used in calculations, the well-known scalar parameters g_x, g_y, g_z, D and E are reported in the tables of results and an explanation of the notation used is necessary. The zero-field splitting part (terms with D and E) of eq 2 can also be expressed by using the zero-field splitting tensor {**D**}:

$$\hat{\boldsymbol{H}}_{zfs} = \hat{\boldsymbol{S}}\,\{\mathbf{D}\}\,\hat{\boldsymbol{S}} \qquad (5)$$

Analogously, the zfs terms in (3) may be replaced by

$$\hat{\boldsymbol{H}}_{zfs} = \hat{\boldsymbol{S}}_1\,\{\mathbf{D}_{12}\}\,\hat{\boldsymbol{S}}_2 \qquad (6)$$

The relation between $\{\mathbf{D}_{12}\}$ and {**D**} is similar to eq 4 (again, in a dimer of S=1/2 ions only):

$$\{\mathbf{D}_{12}\} = 2\,\{\mathbf{D}\} \qquad (7)$$

In a system of coordinates in which the {**D**} tensor is diagonal, the relations between the diagonal tensor elements D_{xx} etc. and the scalar parameters D and E are

$$D = (2D_{zz} - D_{xx} - D_{yy})/2 \;\text{ and }\; E = (D_{xx} - D_{yy})/2 \qquad (8)$$

Formulas (8) relate in the same way either the diagonal elements of {**D**} to D, E, or the diagonal elements of $\{\mathbf{D}_{12}\}$ to D_{12}, E_{12}. Because all our dimers are centrosymmetric, the g components of the "giant spin" Hamiltonian (2) are equal to the g components of the individual ions. The latter

is not valid for the trinuclear systems (see below), where extracting the g components of individual ions is much more challenging.

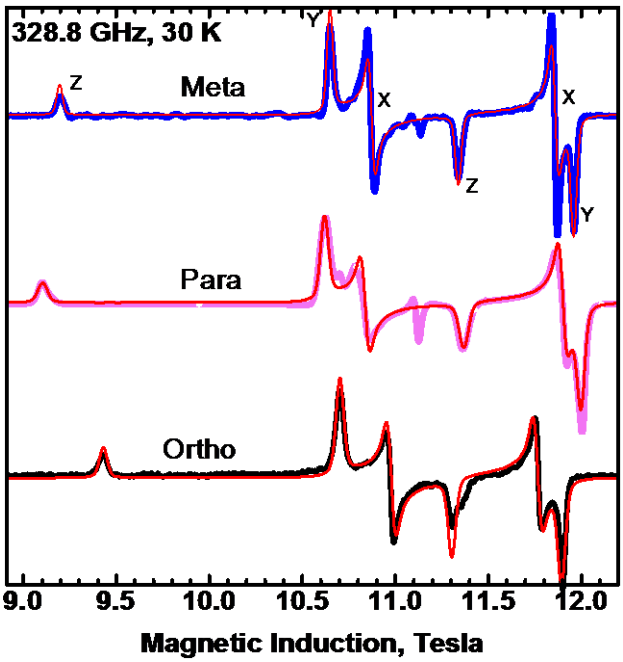

Figure 7. Powder EPR spectra of the dimeric ortho- meta- and para-methoxybenzoato complexes $[Cu_2(H_2TEA)_2(RCOO)_2]\cdot 2H_2O$ recorded at 30 K with the microwave frequency 328.8 GHz. The red traces are simulated with parameters from Table 4 and a 11 deg misalignment between the g matrix and the zfs tensor. Labels x, y, z indicate the molecular orientations at which transitions occur.

Table 4. Experimental Spin Hamiltonian parameters and estimated anisotropic exchange contributions to the zero-field splitting, D_{ex}, and E_{ex}, for the dinuclear complexes $[Cu_2(H_2TEA)_2(RCOO)_2]\cdot 2H_2O$

R	J, cm^{-1}	$g_x = g_y$	g_z	D, cm^{-1}	E, cm^{-1}	D_{ex}, cm^{-1} [a]	E_{ex}, cm^{-1} [a]
m-$OCH_3C_6H_4$	101 [b]	2.064	2.311	-1.066	-0.0393	-1.13	0.01
o-$OCH_3C_6H_4$	-83 [b]	2.064	2.291	-0.907	-0.0495	-0.97	0
p-$OCH_3C_6H_4$	101 [b]	2.063	2.318	-1.140	-0.0393	-1.20	0.01
C_4H_3O [c]	-	2.060	2.305	-1.075	-0.0374	-1.14	0.01
$NO_2C_6H_4$	100 [d]	2.060 [d]	2.303 [d]	-1.135 [d]	-0.0430 [d]	-1.20	0.01

[a] D_{ex} and E_{ex} were obtained by subtracting D_{dip} = 0.06 cm^{-1} and E_{dip}= -0.05 cm^{-1} from the experimental D and E (see below). [b] Ref. 8. [c] This work, observed as a contamination in a trinuclear complex sample. [d] Ref. 28

Table 4 lists the g components and zero-field splitting parameters *D* and *E* for the dimeric complexes together with the exchange integrals. Parameters of a dimer derived from nitrobenzoic acid and TEA[28] are also given for comparison. Although no pure dimer could be obtained in the furanoic acid system, it was observed as a contamination in a less successful preparation of the corresponding trinuclear complex (Fig. S1 in SI) and its EPR parameters were determined.

High-Field EPR offers a possibility of determination of the sign of the zero-field splitting parameters as it affects the intensity pattern in the low temperature spectra.[8,29] Negative *D* was found for all dimeric complexes studied in this work. The g and *zfs* parameters of the ferromagnetic dimers in Table 4 span a rather narrow range and are also not much different for the one antiferromagnetic dimer. Interestingly, for a successful EPR simulation, 11 deg rotation of the g matrix about the y axis of the *zfs* tensor must be assumed for each dimer in Table 4. With this rotation, the spectra at any microwave frequency can be simulated with the same set of the g, *D* and *E* parameters.

EPR Spectra and Magnetic Susceptibility of Trinuclear Complexes

Spectra of the three centrosymmetric trimers **1**, **2** and **3**, as well as of AWEQEZ[12] (spectrum shown in Fig. S2 of SI) are qualitatively similar, but show considerable variations in the zero-field splitting parameters (Table 5). All exhibit small *E*/*D* ratio, opposite to the asymmetric complex **4**, for which *E*/*D* is close to 1/3 (see below). Spectra of complexes **3** and **4**, which are both meta-methoxybenzoates, are compared in Fig. 8. Figure 9 shows the thermal dependence of the effective magnetic moment for compounds **1-4**. The effective magnetic moment at room temperature is ca. 3.4 BM, which is slightly larger than expected for three isolated Cu(II) ions, (expected $(3/2)g_{ave}$, thus some 3.2 BM with a reasonable $g_{average}$ of 2.15). Upon temperature lowering, the magnetic moment increases to a maximum of 4.12 - 4.18 BM corresponding to full occupation of the coupled S=3/2 state - expected $g_{ave}\sqrt{(15/4)} = 4.16$. The interactions are thus of ferromagnetic character. At the lowest temperatures, the magnetic moment falls slightly due to the splitting of the ground S=3/2 state by the Zeeman and zero-field splitting interactions. The magnetic moment is slightly lower for **4** than for other ones (Fig. 9). Since the parameters

derived from EPR were used to interpret the magnetic data, the EPR spectra will be discussed first.

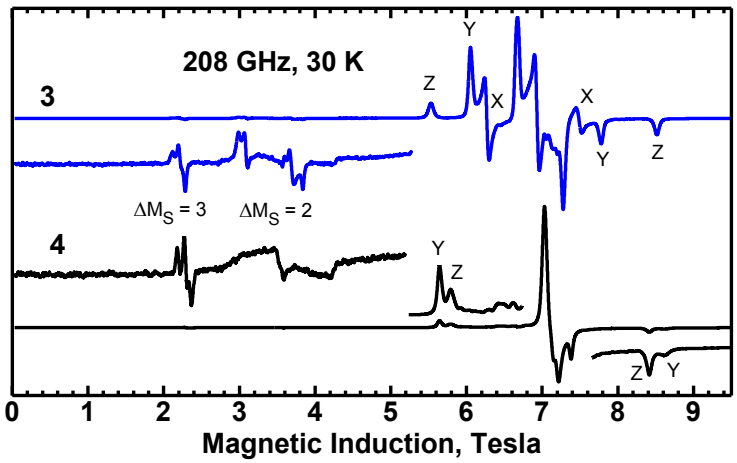

Figure 8. HF EPR spectra of the symmetric complex **3** and the non-symmetric complex **4** recorded at 30 K with the microwave frequency 208.00 GHz. The magnified traces show the 'forbidden' $\Delta M_S = 2$ and $\Delta M_S = 3$ transitions appearing at roughly ½ and 1/3 of the normal resonance field, respectively. Labels X, Y and Z indicate the molecular orientations at which the respective 'allowed' transitions occur.

Table 5. The coupled-spin Hamiltonian parameters for the trinuclear complexes

Complex	J_{12}, J_{23} cm^{-1} [a]	g_x [b]	g_y [b]	g_z [b]	D,[b] cm^{-1}	E,[b] cm^{-1}	α, β, γ,[c] deg
1	77.1(5), -1.2(4)	2.236	2.145	2.070	0.686	-0.014	9, 40, -25
2	66.4(6), -6.8(4)	2.225	2.123	2.065	0.977	0.035	6, 35, -19
3	59.5(6), -6.8(4)	2.222	2.124	2.058	0.724	0.039	9, 37, -18
4	51(1), -4.7(6)	-	2.15[d]	2.09 [d]	0.64 [d]	0.23 [d]	-
AWEQEZ [e]	66, 0[e]	2.228	2.133	2.067	0.710	-0.033	8, 40, -23

[a] J values refer to the spin Hamiltonian (9). [b] g, D and E values refer to the coupled-spin Hamiltonian (2) with S=3/2. [c] Main axes of the coupled {**g**} matrix were obtained by consecutive rotations of the main axes of the *zfs* tensor by angles α, β and γ, about the x, y and z axes, respectively. [d]Powder EPR spectra could not be simulated, parameters determined from the frequency dependencies of the resonance positions (Fig. S4). [e]J value taken from Ref 12. (HF EPR spectrum shown in Fig S2).

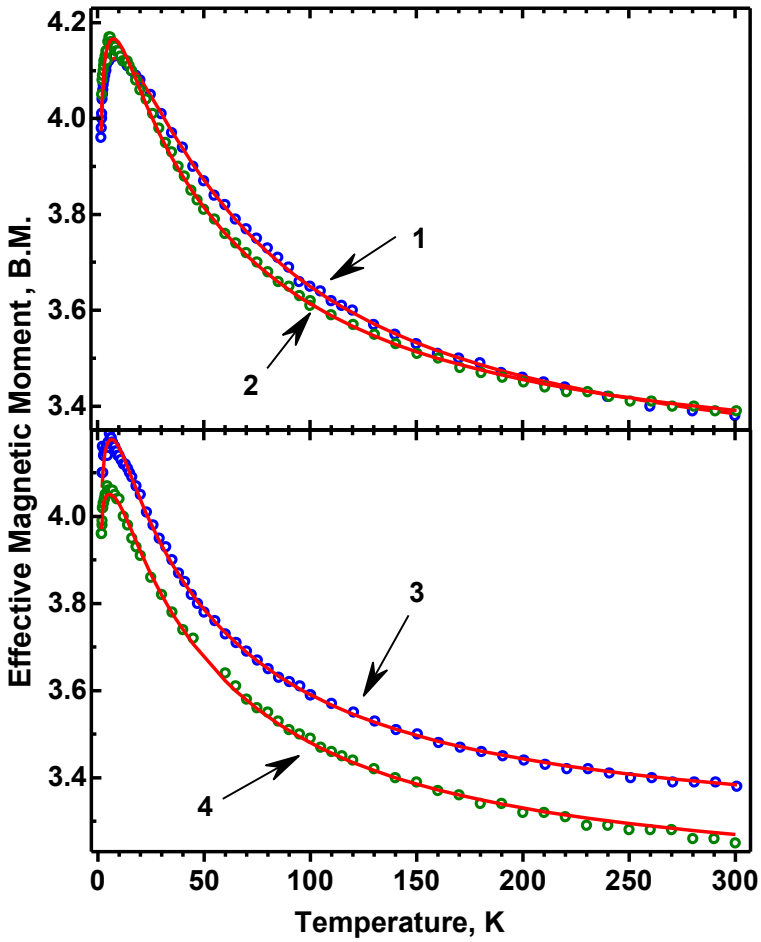

Figure 9. The magnetic properties of complexes **1**, **2**, **3** and **4**. Circles are the experimental data and red lines are calculated with the J_{12} and J_{23} parameters from Table 5. The $D_{12} = D_{13}$, $E_{12} = E_{13}$ parameters of spin Hamiltonian (9) were obtained by multiplying the "giant spin" Hamiltonian parameters D and E, as found from EPR (Table 5) by 3. In the magnetic data fitting, $g_{average}$ was allowed to vary and values of 2.136, 2.163, 2.167 and 2.085 were obtained for **1**, **2**, **3**, and **4**, respectively. No intermolecular interactions needed to be taken into account in the cases of **1**, **2**, and **3**. For **4**, the fit was significantly improved with the zJ parameter of 0.037 cm^{-1}.

Spin Hamiltonian parameters for the centrosymmetric trinuclear complexes.

Out of our four trinuclear complexes, two (**1** and **2**) possess the inversion center and a third one (**3**) is very close to having one and will be also treated as centrosymmetric. The terminal copper ions (2 and 3) in the centrosymmetric systems are equivalent, the corresponding main axes of their {**g**} matrices are parallel and the corresponding g components of ions 2 and 3 are equal, like $g_{2x} = g_{3x}$ etc. Also, both the isotropic and anisotropic interactions 1-2 and 1-3 must be equal. The spin Hamiltonian, which can be used to interpret both the magnetic and EPR data is[27]

$$\hat{H} = \quad -J_{12}(\hat{\mathbf{S}}_1\,\hat{\mathbf{S}}_2 + \hat{\mathbf{S}}_1\,\hat{\mathbf{S}}_3) - J_{23}\hat{\mathbf{S}}_2\,\hat{\mathbf{S}}_3 + \\ + \hat{\mathbf{S}}_1\{\mathbf{D}_{12}\}\,\hat{\mathbf{S}}_2 + \hat{\mathbf{S}}_1\{\mathbf{D}_{13}\}\,\hat{\mathbf{S}}_3 + \hat{\mathbf{S}}_2\{\mathbf{D}_{23}\}\,\hat{\mathbf{S}}_3 \qquad (9) \\ + \mu_B B\{\mathbf{g}_1\}\,\hat{\mathbf{S}}_1 + \mu_B B\{\mathbf{g}_2\}\,\hat{\mathbf{S}}_2 + \mu_B B\{\mathbf{g}_3\}\,\hat{\mathbf{S}}_3$$

where $\{\mathbf{g}_i\}$ represent the g matrices and $\{\mathbf{D}_{ij}\}$ are the zero-field splitting tensors for the appropriate pairs.

The first line in eq 9 is the Heisenberg Hamiltonian that describes the isotropic part of the metal-metal interactions. The eigenstates of this Hamiltonian are two doublet states D_1 and D_2 with S_T=1/2 and a quartet state Q, (S_T=3/2). S_T is the total spin of the system, $\hat{\mathbf{S}}_T = \hat{\mathbf{S}}_1 + \hat{\mathbf{S}}_2 + \hat{\mathbf{S}}_3$. The relative energies can be expressed by J_{12} and J_{23} as:

$$E(D_1) = 3J_{12}/2$$
$$E(D_2) = J_{12}/2 + J_{23} \qquad (10)$$
$$E(Q) = 0$$

These energies determine the bulk magnetic properties. For EPR, on the other hand, the anisotropic metal-metal interactions and the Zeeman term (lines 2 and 3 in eq 9, respectively) are decisive.

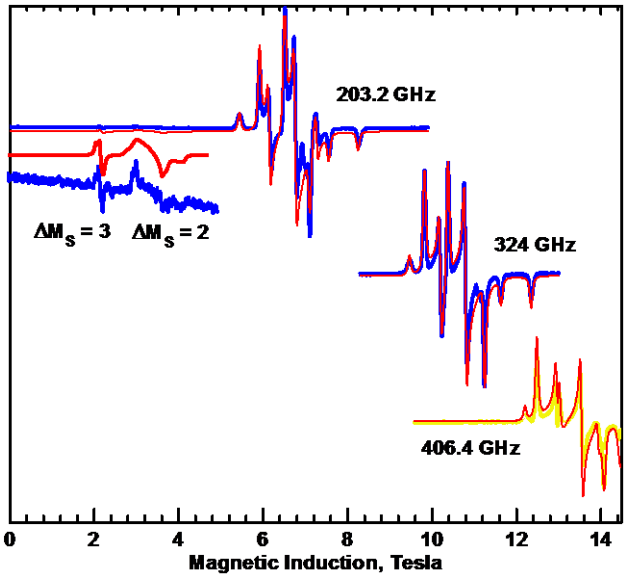

Figure 10. Experimental (blue) EPR spectra of **1** recorded at 30 K with the microwave frequencies as marked. Red: spectra simulated using spin Hamiltonian (2) with S=3/2 and parameters given in Table 5. The magnified traces in the top spectrum show the "forbidden" transitions, ΔM_S=2 and 3 which appear at roughly 1/2 and 1/3 of the magnetic induction in the center of the main spectrum, respectively.

The parameters of spin Hamiltonian (9) are difficult to determine experimentally due to their number and the fact that the matrices are diagonal in different coordinate systems – there are three *g* components for each copper ion and while the main axes of the {**g**} matrices for the terminal ions 2 and 3 are parallel and their main values are equal, those for the central ion 1 are different. Because of the inversion symmetry in three of our trimers **1**, **2**, and **3** (approximate), the main axes of the two *zfs* tensors, $\{\mathbf{D}_{12}\}$ and $\{\mathbf{D}_{13}\}$ are parallel, but their absolute orientation is unknown. Also, Hamiltonian (9) operates in the space of eight spin functions of a trinuclear copper(II) system. In our case, the isotropic exchange interactions are strong and the ground quartet state is well separated from the excited doublets. We will therefore first use the "giant spin" approach, meaning that only the quartet state will be considered and spin Hamiltonian (2) with S=3/2, operating within a space of only 4 spin functions will be applied, which greatly shortens the time of the powder EPR spectra simulations.

Such simulations for compounds **1-3** are presented in Figs. 10, 11 and 12**,** respectively and the spin Hamiltonian parameters are given in Table 5. For a successful simulation, the $\{\mathbf{g}\}_Q$ matrix main axes had to be rotated versus the zfs tensor main axes. That transformation was accomplished by three consecutive rotations by angles α, β, γ about the x, y and z axes of {**D**}, respectively. The rotation angles are given in Table 5. Positive sign of *D* was found in each case.

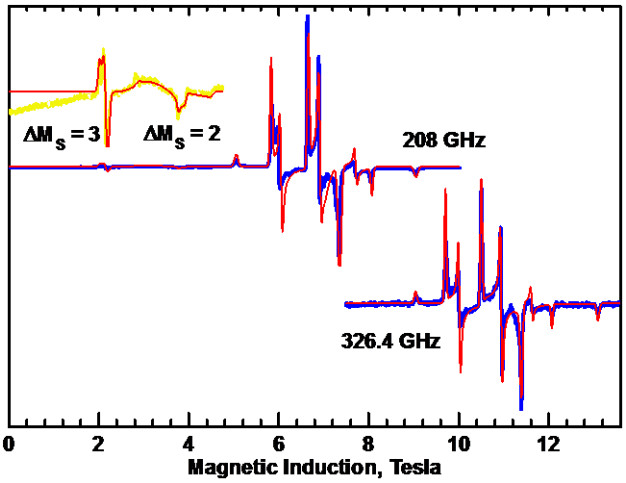

Figure 11. Experimental (blue) EPR spectra of **2**. Red: simulated by using spin Hamiltonian (2) with parameters in Table 5. The magnified traces show the "forbidden" transitions in the 208 GHz spectrum.

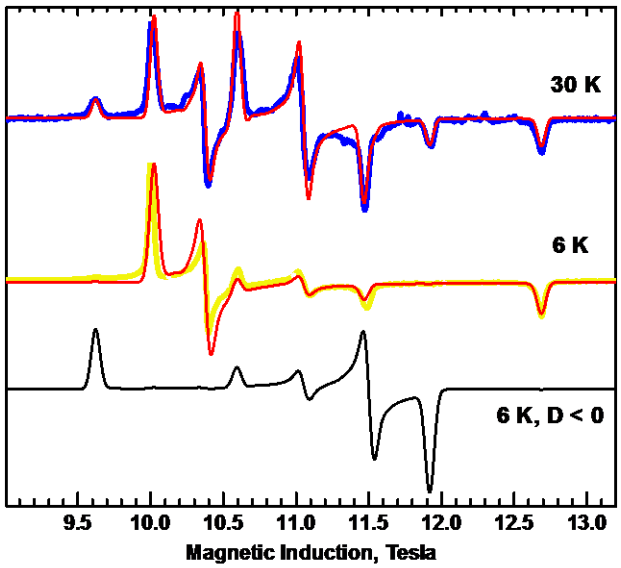

Figure 12. Blue: Spectra of **3** recorded with ν = 328.8 GHz at 30 K (top) and 6 K (center). Red: simulated by using spin Hamiltonian (2) with parameters in Table 5. The bottom trace is a simulated 6 K spectrum with the sign of D and E inverted.

The *g* values in Table 5 do not seem correct for copper(II) in square planar coordination. It is important to understand that they are pertinent to the coupled-spin Hamiltonian (2) and are combinations of the *g* factors of separate copper ions. In a trinuclear Cu(II) system, the $\{\mathbf{g}_i\}$ matrices combine differently (Table 4.4 in ref 27) in the D_1, D_2 and Q states (which were defined in Eq 10):

$$\{\mathbf{g}\}_Q = (\{\mathbf{g}_1\} + \{\mathbf{g}_2\} + \{\mathbf{g}_3\})/3$$
$$\{\mathbf{g}\}_{D1} = (2\{\mathbf{g}_2\} - \{\mathbf{g}_1\} + 2\{\mathbf{g}_3\})/3 \qquad (11)$$
$$\{\mathbf{g}\}_{D2} = \{\mathbf{g}_1\}$$

Indexes 2 and 3 refer to the terminal copper ions, while 1 is for the central one. Since $\{\mathbf{g}_2\}$ is parallel to $\{\mathbf{g}_3\}$, but $\{\mathbf{g}_1\}$ is oriented differently, a transformation of $\{\mathbf{g}_2\}$ to the main axes of $\{\mathbf{g}_1\}$ must be performed before eqs 11 can be applied. In this work, no EPR signals attributable to either D_1 or D_2 states were observed at any temperature. EPR spectrum of the D_1 state, with peculiar g components resulting from eq 11, was observed in Refs. 30, where D_1 was the ground state of the antiferromagnetic trinuclear copper complexes. The $\{\mathbf{g}\}$ matrix orientation in a square planar Cu(II) complex is predictable – the Z axis (largest g component) is expected to be perpendicular to the plane of the equatorial ligand atoms. The terminal copper atom environment in our trinuclear systems is similar to that of the copper atoms in the dimeric complexes, thus their g components (Table 4) may be expected to be similar. The $\{\mathbf{g}\}$ matrices of interacting

atoms in dimers are parallel, therefore the g components in the triplet spin state are the same as the g components of individual ions. Hence, at this point we can assume that we approximately know the $\{\mathbf{g}_2\} = \{\mathbf{g}_3\}$ matrix for the terminal copper atoms. From the EPR simulations in the "giant spin" regime, the orientation of the coupled $\{\mathbf{g}\}_Q$ matrix versus the coupled $\{\mathbf{D}\}$ tensor in the quartet state is also known *via* the angles α, β, γ (Table 5). The following procedure was devised to extract the g parameters of the central copper: The expected main axes of $\{\mathbf{g}_1\}$ (central Cu atom), with the Z axis perpendicular to the plane of four equatorial oxygen atoms were used as the main system of coordinates. The $\{\mathbf{g}_1\}$ matrix was assumed axial, i.e. $g_{1x} = g_{1y}$. The main axes of $\{\mathbf{g}_2\}$ (terminal Cu atoms) were chosen with the Z axis perpendicular to the OOON plane. Now, the values of $g_{1x} = g_{1y}$ and g_{1z} were chosen, the $\{\mathbf{g}_2\}$ matrix was transformed into the system of $\{\mathbf{g}_1\}$, resulting in a non-diagonal matrix which was added to the diagonal $\{\mathbf{g}_1\}$ matrix to obtain $\{\mathbf{g}\}_Q$ according to eq 11. The latter matrix was finally diagonalised and such $g_{1x} = g_{1y}$ and g_{1z} values were sought which when subject to the above procedure would result in the g_x, g_y and g_z of the quartet state as determined before from the "giant spin" method (Table 5). This procedure also yields the main axes of $\{\mathbf{g}\}_Q$ expressed in the main axes system of $\{\mathbf{g}_1\}$ (see Fig 13). But since the orientation of $\{\mathbf{D}\}$ versus $\{\mathbf{g}\}_Q$ is known, the orientation of $\{\mathbf{D}\}$ versus $\{\mathbf{g}_1\}$ can now be calculated. Some tweaking of the $\{\mathbf{g}_2\}$ components was required, but finally they were not significantly different from those of the dimers. The final diagonal $\{\mathbf{g}_1\}$ components were slightly larger than those of $\{\mathbf{g}_2\}$ in agreement with the equatorial O_4 coordination of the central copper ion versus O_3N for the terminal ones (see Fig 14 caption). With the spatial relations between $\{\mathbf{D}\}$, $\{\mathbf{g}_1\}$ and $\{\mathbf{g}_2\}$ found in the above way, we can turn back to spin Hamiltonian (9) and simulate the EPR spectra in the non-coupled representation using all 8 spin functions in the system. In a trinuclear system of S=1/2 ions, the zero-field splitting parameters for the interactions 1-2 and 2-3, D_{12}=D_{23} and E_{12}=E_{23} are related to the D and E parameters of the "giant spin" Hamiltonian (2):[27]

$$D_{12} = 3\,D, \quad E_{12} = 3E \qquad (12)$$

Parameters D_{12} and E_{12} were converted to the $\{\mathbf{D}_{12}\}$ tensor using eq 8. Tensors $\{\mathbf{D}_{12}\}$ and $\{\mathbf{D}_{13}\}$ are identical due to symmetry and the anisotropic interactions 2-3 were neglected. The simulating program used the $\{\mathbf{g}_1\}$ main axes as the system of coordinates. The $\{\mathbf{g}_2\} = \{\mathbf{g}_3\}$ matrices and the $\{\mathbf{D}_{12}\} = \{\mathbf{D}_{13}\}$ tensors were rotated to that system of axes.

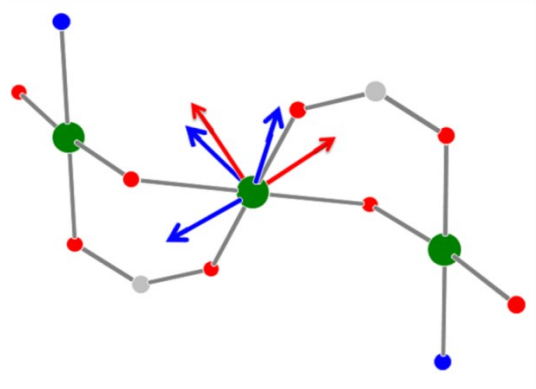

Figure 13. The skeleton of the trimeric complex **1**. The red arrows represent the directions of the main axes of the zfs tensor and the blue arrows show the coupled $\{\mathbf{g}\}_Q$ matrix orientation. The view is along D_{xx}.

The complex 8x8 matrix of spin Hamiltonian (9) was diagonalised numerically and the EPR resonances at a molecular orientation were found by an iterative procedure. A powder spectrum was simulated as a superposition of spectra calculated at very large number of molecular orientations. The resulting simulation (Fig 14 for **1**) is not perfect but shows that the assumptions above are essentially correct. The discrepancies may be due to assumptions regarding the axiality of the $\{\mathbf{g}\}$ matrices, their orientation in space and neglecting the anisotropic interactions 2-3. The same procedure applied to **2** and **3** resulted in simulations with the use of spin Hamiltonian (9) of similar quality as that in Figure 14. The simulations using the "giant spin" Hamiltonian were very successful for **1**-**3** and AWEQEZ (Fig. S2).

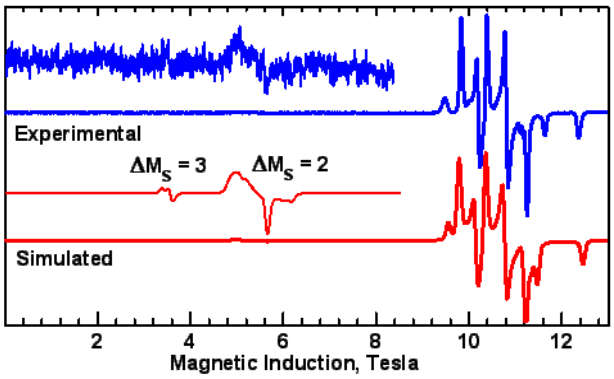

Figure 14. EPR spectra of **1**. Top: experimental, 30 K, 324.0 GHz. Bottom: simulated using spin Hamiltonian (9) with $J_{12} = J_{13} = 78$ cm^{-1}, $J_{23} = -1.2$ cm^{-1}, $g_{1x} = g_{1y} = 2.07$, $g_{1z} = 2.35$, $g_{2x} = g_{2y} = 2.07$, $g_{2z} = 2.29$, $D_{12} = 2.058$ cm^{-1}, $E_{12} = 0.042$ cm^{-1}. (See text). The magnified traces show the "forbidden" transitions.

Magnetic susceptibility

The spin Hamiltonian in form (9) was used to fit the magnetic susceptibility data. The D_{12} and E_{12} found from EPR were not allowed to vary and were converted to the zfs tensors according to eq 8. Average g value was used rather than individual g components and it was allowed to vary to account for common problems in magnetic susceptibility data, like uncertainty of the effective molar mass at the time of the magnetic measurements. The difference between the average $g_{magnetic}$ and g_{EPR} was -0.014, 0.026, 0.032 and -0.065 for **1**, **2** **3** and **4**, respectively, which should be considered a very good agreement at least in the first three cases. The exchange integrals J_{12}=J_{13} and J_{23} were allowed to change.

The spin Hamiltonian (9) matrix was diagonalised to find the energy levels and the magnetic susceptibility per mole at a molecular orientation given by polar angles Θ, Φ was calculated from

$$\chi(\Theta,\Phi) = -\frac{N}{B}\frac{\sum_{i=1}^{8}\frac{\partial E_i}{\partial B}\exp(-E_i/kT)}{\sum_{i=1}^{8}\exp(-E_i/kT)} \qquad (13)$$

The derivatives of the energies E_i with respect to the magnetic field B, $\partial E_i/\partial B$ can be evaluated numerically by calculating the energy levels slightly below and slightly above (±5 Gauss) the operational magnetic field of a SQUID magnetometer (B = 5000 G in our case). The powder susceptibility was calculated by numerical integration of $\chi(\Theta,\Phi)\sin\Theta d\Theta d\Phi$. When the zero-field and Zeeman splitting have been taken into account in this way, the magnetic properties were reproduced adequately without a need of considering intermolecular interactions. However, for **4** the fit is better when they are allowed.

The electronic spectra and the EPR g values

In the reflectance spectra of all dinuclear and trinuclear complexes, (Figure S8), the d-d transitions which are related to the EPR g parameters were observed at 13300 cm^{-1} (xy → x^2-y^2) and 15700 cm^{-1} (xz, yz → x^2-y^2). Relations between those transitions and the g parameters are

$$g_z = 2.0023 - \frac{8\lambda}{E_{x^2-y^2} - E_{xy}}$$
$$g_{x(y)} = 2.0023 - \frac{2\lambda}{E_{x^2-y^2} - E_{yz(xz)}} \qquad (14)$$

The spin-orbit coupling constant λ= - 828 cm^{-1} for Cu^{2+} is reduced in covalent compounds due to electron delocalization. DDCI calculations on the quartet ground state (below) indicate that the unpaired electron density on the copper ions of complex **1** is 0.668 on Cu1 and 0.556 on Cu2. When λ is reduced by these densities to -553 and -460 cm^{-1} for Cu1 and Cu2, respectively, the above formulas result in g_z = 2.33 and 2.28, respectively, in reasonable agreement with the experimental data (Fig 14 caption). The $g_{x,y}$ values estimated in this way are 2.07 for Cu1 and 2.06 for Cu2. Owing to very limited resolution of the electronic spectra, the above numbers must be treated as rough approximations.

The non-centrosymmetric complex 4

The EPR spectra of **4** are seemingly simpler than the spectra of **1**, **2** and **3**, but they could not be simulated even when using just the "giant spin" approach. A likely reason for this problem is the antisymmetric exchange (Dzialoshinskii-Moriya) interaction,[31]

$$\hat{\boldsymbol{H}}_{\boldsymbol{DM}} = \boldsymbol{d} \bullet (\hat{\boldsymbol{S}}_{\boldsymbol{i}} \times \hat{\boldsymbol{S}}_{\boldsymbol{j}}) \qquad (15)$$

which is only possible in a system lacking the inversion center. That interaction adds three new parameters – the Moriya vector ***d*** components to each of the interactions 1-2 and 1-3, and with the lack of a symmetry relation between the interactions 1-2 and 1-3, the problem becomes unmanageable. Fortunately, the splitting between the Kramers doublets |±1/2> and |±3/2> of the quartet state could still be determined by analyzing the high-field EPR spectra recorded with various microwave frequencies (Fig. S4). The EPR transition between the |±3/2> and |±1/2> Kramers doublets occurs at zero magnetic field when the microwave frequency is ~45 GHz, which immediately gives the splitting Δ between these Kramers doublets of ~1.5 cm^{-1}. Δ is related to the D and E parameters (of the giant spin Hamiltonian) by $\Delta = 2\sqrt{D^2 + 3E^2}$. Moreover, the form of the high-field spectra, in which the "Z" and "Y" resonances are close to overlap, indicates that E is close to D/3 in this complex, which is often referred to as the maximum rhombicity case. Analysis of the frequency dependencies (see SI) led to D = 0.64 cm^{-1}, E = 0.23 cm^{-1} (Table 5), and these values were used in fitting of the magnetic data. An additional complication is that opposite to complexes **1** - **3**, the two central to terminal interactions J_{12} and J_{13} need not be equal, which is nicely shown by the theoretical calculations (see below). For comparative purposes, complex $[Cu_3(C_6H_5CO_2)_4\{(C_2H_5)_2NC_2H_4O\}_2H_2O]$ (**6** in ref 10f) was synthesized. That complex possesses no inversion center, like **4**, but has a two-fold axis passing

through the central copper ion. A spectrum similar to that of **4** was obtained (Fig. S5), exhibiting a larger Δ of some 2.0 cm^{-1} and a high E/D ratio. Similarly as in the case of **4**, no full EPR simulation was possible despite of the higher symmetry.

Comparison to the literature EPR and magnetic data of similar systems

The linear trinuclear complexes similar to ours were reported in many papers.[10-13] While X-band EPR (~9.5 GHz) has mainly been applied, we found some papers reporting the HF EPR spectra.[10a,b] Surprisingly, no determination of the zero-field splitting parameters from HF EPR data was attempted. In X-Band EPR typically a resonance close to the effective g = 4.3 value is observed, accompanied by another one close to g_{eff} of 2.1.The former one is due to transitions within the |±1/2> Kramers doublet of the S=3/2 state, at the "perpendicular" orientation. The appearance of that feature indicates that the splitting between the Kramers doublets of the S=3/2 state is larger than the microwave quantum energy. The g_{eff} = 2.1 signal is a combination of transitions within the |±1/2> Kramers doublet of S=3/2 at the "parallel" orientation and those occurring within the excited S=1/2 state(s). In some cases, the g=4.3 signal was observed to shift towards the g=2.1 position when temperature was increased from 4.2 K to 80 K and above, which was explained by coalescence of the resonances due to the quartet and doublet states[10a,e,13]. In the X-Band spectra of our trinuclear complex **1**, those g=4.3 and g=2.1 signals are observed (Figure 15) , but do not coalesce at higher temperatures, similarly as was observed in the very closely structurally related thiophenylcarboxylate-TEA trimer,[12] meaning that there is no fast relaxation between the ground state and the excited doublet states. No coalescence effects are expected in our high-field spectra in which transitions between the |±3/2> and |±1/2> Kramers doublets are observed, allowing accurate determination of the D and E parameters. We have synthesized for comparative purposes complex $[Cu_3(thiophenyl\text{-}COO)_4(H_2TEA)_2]$ (AWEQEZ) for which D = 0.83 cm^{-1} and $g_{average}$=2.16 were determined from magnetic data.[12] That compound is isostructural with **1**. Analysis of its HF EPR spectra in this work (Fig. S2) led to D = 0.710 cm^{-1}, E= -0.033 cm^{-1} and also allowed determination of the relative orientation of the {D} tensor versus the {g} matrix (Table 5).

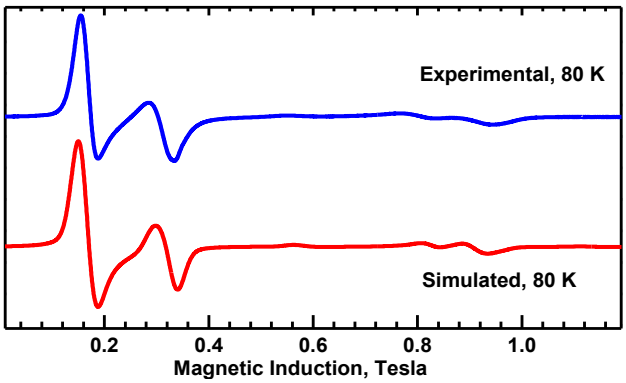

Figure 15. X-Band EPR spectrum of **1**, recorded at 80 K. The spin Hamiltonian [9] parameters determined from the high-field spectra recorded at 30 K were used in the simulation. Compare to the high-field spectra of **1** (Figs 10 and 14).

The magnetic properties of many trinuclear copper complexes similar to ours have been reported.[10-13] In cases where only the J_{12} interaction has been considered, its magnitude has been found to be around 60-90 cm^{-1}.[11,12,13] When allowing non-zero J_{23} (terminal to terminal interaction) in the fitting procedures, it has always been found antiferromagnetic,[10a,d-f] in agreement with our experimental results. Sometimes, the magnitude of J_{23} was a surprisingly large fraction of J_{12}, like 20%.[10e] In our complexes, attempts of forcing in the magnetic fitting J_{23} to positive values (ferromagnetic), or just to zero, caused a visible deterioration of the average deviation of the calculated magnetic data from the experimental ones. Moreover, the deviations took a systematic character being positive at low temperatures and negative at higher. This effect could not be compensated by assuming intermolecular interactions. The experimental results, both ours and those in the literature, thus hint at the antiferromagnetic character of J_{23}, although the intuition and the theoretical calculations presented below indicate otherwise.

The nature of the zero-field splitting

In polynuclear copper(II) complexes there are two contributions to the zero-field splitting, one of which is caused by the magnetic dipole-dipole interaction and the other one is due to the anisotropic exchange interactions:[27-29]

$$D = D_{ex} + D_{dip},\ E = E_{ex} + E_{dip} \qquad (16)$$

The theory of the latter has been in progress recently.[32] To estimate the exchange contribution, the dipolar part must be subtracted from the experimental zfs parameters (see last 2 columns of

Table 4). The largest component of the dipole-dipole interaction tensor is along the Cu-Cu direction, while the largest component of the exchange-related zfs interaction is expected to be parallel to the direction of g_z,[27-32] which in our dimeric complexes is roughly perpendicular to the Cu-Cu vector. When that direction is labeled "Z" and that of the C-Cu vector is "X" then the expressions for D_{dip} and E_{dip} (referred to the giant spin Hamiltonian) are[33]

$$D_{dip} = (2g_z^2 + 2g_x^2 - g_y^2)\mu_B^2/4R^3_{Cu\text{-}Cu} \qquad (17)$$

$$E_{dip} = -(2g_x^2 + g_y^2)\mu_B^2/4R^3_{Cu\text{-}Cu}$$

These formulas are approximate, as they do not take into account the electron delocalization. A strong effect of delocalization was observed in a biradical system, in which the point dipole D_{dip} was too small compared to the experiment, while the value obtained by using the wavefunction was correct.[34] The effect was less pronounced for the dimeric copper acetate, where the point-dipole D_{dip} = -0.17 cm^{-1} was too large[29] compared to the quantum-mechanical value of -0.12 cm^{-1}.[32a] Because of the approximate character of eq 17 and close similarity of both the structures and the *g* parameters of all our dimeric complexes, we will use for all of them the same D_{dip} = 0.06 cm^{-1} and E_{dip} = -0.05 cm^{-1}, which result from eq 17 with $R_{Cu\text{-}Cu}$ of 2.92 Å. It is thus seen that the dipolar contribution is minor compared to the overall *D* of -1 to -1.2 cm^{-1} (Table 4), and that the zero-field splitting related to the anisotropic exchange is almost axial ($E_{ex} << D_{ex}$). The exchange interaction anisotropy is caused by mixing of the excited states of a system to its ground state *via* the spin-orbit coupling.[27,32] An excited state can only contribute to zfs if a non-zero matrix element of the **L** operator exists between that excited state and the ground state.[27,32] The excited states of a pair to be considered in our complexes are those in which one of the copper ions is in its ground state $d_{x^2-y^2}$ while another one is in an excited state – d_{xy}, d_{xz} or d_{yz}. In the dimeric copper(II) complexes with the $d_{x^2-y^2}$ ground state, D_{ex} and E_{ex} can be expressed as[32a]

$$D_{ex} = 2\frac{\lambda^2 J_{x^2-y^2,xy}}{\Delta E^2_{x^2-y^2,xy}} - \frac{1}{4}\frac{\lambda^2 J_{x^2-y^2,xz}}{\Delta E^2_{x^2-y^2,xz}} - \frac{1}{4}\frac{\lambda^2 J_{x^2-y^2,yz}}{\Delta E^2_{x^2-y^2,yz}} \qquad (18)$$

$$E_{ex} = \frac{1}{4}\frac{\lambda^2 J_{x^2-y^2,xz}}{\Delta E^2_{x^2-y^2,xz}} - \frac{1}{4}\frac{\lambda^2 J_{x^2-y^2,yz}}{\Delta E^2_{x^2-y^2,yz}}$$

where the symbols $J_{x^2-y^2,n}$ are the exchange integrals between the $d_{x^2-y^2}$ ground orbital of one copper ion and an excited d_n orbital of another, and λ = -828 cm^{-1} is the spin-orbit coupling constant for Cu^{2+}. The exchange integrals $J_{x^2-y^2,xz}$ and $J_{x^2-y^2,yz}$ are expected to be similar, as may

be inferred from Fig. 16 which shows the arrangement of these orbitals. Also, $\lambda/\Delta E_{x^2-y^2,xz}$ and $\lambda/\Delta E_{x^2-y^2,yz}$ must be equal because g_x and g_y are equal (eq 14). Accordingly, the E_{ex} parameter is expected to be small (eq 18) in agreement with the data in Table 4. The exchange-related zfs interaction is thus axial ($E << D$) and the dipole-dipole interaction is axial as well, but because they operate in different systems of coordinates, their sum is not axial. The experimental E for dimers of this type cannot thus be equal to zero (Table 4). The situation is very different in the well-known dimeric 'paddlewheel' copper carboxylates, in which both the exchange-related and dipole-dipole zero-field splitting have their largest component along the Cu-Cu direction resulting in very small E values.[29] (See also Table S3). On the contrary, very large E values, comparable to D were observed in dinuclear complexes containing copper ions in trigonal bipyramide environment and d_{z^2} ground state. This was explained by the difference between the exchange integrals $J_{z^2,xz}$ and $J_{z^2,yz}$ which determine D_{ex} and E_{ex} in those compounds.[35]

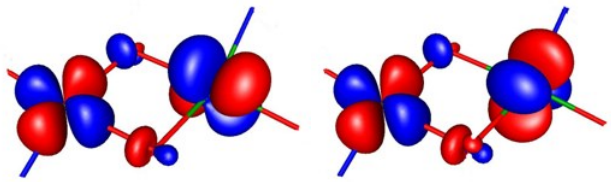

Figure 16. The orbital arrangement in the bridge unit of the dimeric complexes. Interactions between the $d_{x^2-y^2}$ orbital of one ion and d_{xz} of another (left) is expected to be similar to the interaction $d_{x^2-y^2} - d_{yz}$ (right). The Z axis (direction of g_z) is perpendicular to the bridge plane.

The situation in the trinuclear systems is much more difficult. The g matrix axes of the central copper ion are not parallel to the g axes of the terminal atoms, complicating calculations of the dipole-dipole related zfs. In view of the approximate character of the point-dipole model, this is not a major problem. The D_{dip} for interaction 1-2 calculated along the Cu1-Cu2 direction (referred to spin Hamiltonian 9) is -0.18 cm^{-1}, and together with interaction 1-3 it will contribute just -0.06 cm^{-1} to the giant-spin D parameters in Table 5 (see also eq 12). Again, this is a minor contribution, and similarly as in the dimers, the anisotropic exchange must be responsible for most of the zfs. The exchange-related zero-field splitting in pairs Cu1-Cu2 and Cu1-Cu3 could be presumably analyzed in the same way as in the copper dimers.[32] To our knowledge, theoretical calculations like those in ref 32a have not been attempted so far for any trinuclear system.

3.4. Theoretical calculations of the isotropic exchange interaction

Calculations of the exchange interactions in our dimers have already been published8 and the following discussion will refer to the trinuclear complexes only. The trimers **1**, **2** and **3** can be formally considered as a linear chain, where each Cu atom presents a square-planar coordination, CuO_3N for terminal metal centers and CuO_4 for the central Cu (Figure 17). In the analysis of the magnetic orbitals, this plane is considered the xy plane in a local axis system with each Cu at the origin and the x and y axis oriented along the Cu-O(N) bonds. The corresponding CuO_3N and CuO_4 planes form an angle of about 70º in **1**, 64º in **2,** and 66.8º, 67.3º in **3** (no exact inversion center). In each case, two protonated O atoms from the TEA molecule complete the metal coordination sphere as axial ligands, except for the central Cu of compound **4**, with only one TEA protonated O atom in axial position with square-planar pyramid coordination.

Each Cu atom bears one unpaired electron, placed on an in-plane Cu 3 $d_{x^2-y^2}$ orbital. Figure 18 shows the active orbitals obtained from a CASSCF(3/3) calculation on the quartet ground state

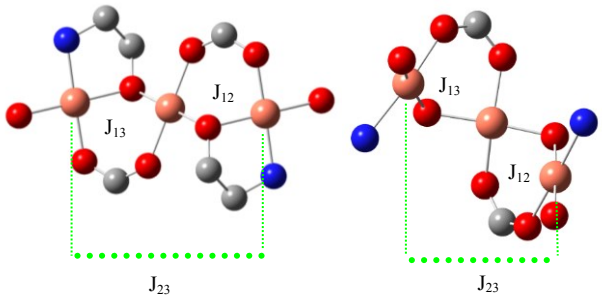

Figure 17. The spin interaction model for **1-3** (left) and **4** (right). The cores are shown containing three Cu atoms and their nearest neighbors.

for the furan derivative **1**, similar shapes are obtained for complexes **2** and **3**. The two terminal CuO_3N planes form a dihedral angle of 180º in **1-3**, and 60º in **4**. The Cu 3d magnetic orbitals on two neighboring centers are quasi-orthogonal (scheme 2), and accordingly, a ferromagnetic coupling between them is expected. In the case of compound **4**, the relative orientation of Cu1 and Cu3 coordination planes is similar to that found in compounds **1-3**, but the plane containing the Cu2 is rotated by 60º with respect to the plane containing the Cu3 center, and a different interaction pattern is expected for this center. The nature and amplitude of the interactions inside these four compounds are analyzed by means of *ab initio* calculations, where both the low-lying

quartet and doublet states are computed, with the aim of identifying the ground state and the energy separations among the states. The magnitude of the magnetic coupling constants between the terminal and central Cu atoms ($J_{12} = J_{13}$) and between the two terminal Cu atoms (J_{23}) will be extracted from the energy difference of the three lowest states, using the relations shown in equation 10. These relations are strictly valid for compounds **1** and **2** where centers Cu2 and Cu3 are related by an inversion centre. We also apply these equations to compound **3**, although it presents a slight deviation with respect to C_i symmetry point group. In compound **4**, Cu2 and Cu3 are no more equivalent (see scheme 3), and three different coupling constants can be distinguished, J_{12}, J_{13} and J_{23}. In this situation, equation 10 just provides a rough estimate of the J values, if any. The rigorous evaluation of the three J values requires combining the two energy differences (equation 10) with the information contained in the wavefunctions by means of an effective Hamiltonian. Details of the procedure can be found in Refs. 36

Usually $|J_{12}| >> |J_{23}|$ and for $J_{12} > 0$, the quartet is the ground state. We have demonstrated in the past that among the available quantum chemistry methods, Dedicated Difference Configuration Interaction (DDCI)[37] is a reliable approach for the evaluation of magnetic coupling constants both in solid state and molecular magnetic systems.[38,39,40,41,42,43,44] The central idea is to build a configuration interaction matrix with all the configurations participating on the energy difference at second-order of perturbation. This excludes all the double inactive excitations (two-electron promotion from the inactive doubly occupied to the virtual empty set of MOs), which are by far the most numerous. The J values obtained in this way are in general in a good agreement with available experimental data.

For the systems considered here, we have selected three active orbitals, which are essentially combinations of the singly occupied Cu 3d atomic orbitals, with delocalization tails on the neighboring atoms. Figures 18 and 19 show the active orbitals for **1** (similar to those of compounds **2-3)** and for **4**, respectively. These three orbitals contain three unpaired electrons and constitute the active space CAS(3/3). Additionally an extended CAS, CAS(7/5), containing also two occupied orbitals centered on the O bridging ligands has been employed.

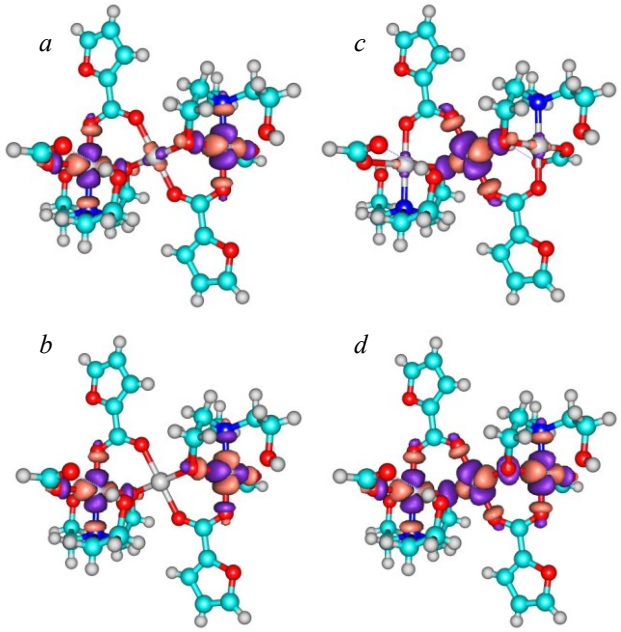

Figure 18. Quartet state active orbitals of complex **1** obtained from a CASSCF(3/3) calculation. "a" and "b" correspond to the symmetric and antisymmetric combinations of the terminal Cu 3d orbitals, with small tails on ligands, "c" is essentially localized on the central Cu atom, and "d" is the sum of the three MOs, to show the relative orientation of the Cu 3d magnetic orbitals.

The energy and wavefunction of the three magnetic states, D_1, D_2 and Q, have been evaluated by means of DDCI calculations on the basis of a minimal CAS(3/3), hereafter DDCI(3/3), and DDCI2 calculations on the extended CAS, referred as DDCI2(7/5). This space contains all the single excitations and the double excitations involving two active orbitals ($occ^2 \rightarrow act^2$ and $act^2 \rightarrow vir^2$).

To reduce the computational cost of the calculations, the two external aromatic rings have been replaced by H atoms (C-H distance of 1.07 Å), while those bonded to the two carboxylate groups are explicitly taken into account. This model retains the intramolecular hydrogen bonds, and maintains the conjugation of the carboxylate C atoms. Difference dedicated molecular orbitals,[45] obtained from the diagonalization of the difference of the CAS+S density matrices of the quartet and the D_1 doublet states, are employed to perform the final calculations. The most important feature of these dedicated MOs is that their eigenvalues can be considered as a measure of the participation of the MO on the description of the magnetic state gaps. By selecting only the most

participating MOs in the subsequent calculations, it is possible to considerably reduce the size of the CI matrix, and hence the diagonalization time, with a negligible effect on the computed energy gaps.[46]

The core electrons of Cu atoms have been represented by means of pseudopotentials, combined with basis set [9s6p6d] with contraction (3s3p4d).[47] Atomic natural orbital (ANO)[48] type basis functions have been used for the rest of atoms, with contractions 4s3p1d for O and C atoms directly connected to metal atoms, 4s3p for O, N and C atoms in the external shell, and 2s for H atoms. MOLCAS 7.8 code[49] has been used for the evaluation of the atomic and molecular integrals and CASDI code[50] for the diagonalization of the CI matrices.

A quartet ground state is found for compounds**1-4**, regardless the level of the calculation, in agreement with the experimental data and the relative orientation of the magnetic Cu 3d orbitals. The energy distribution of the magnetic states is in accordance with a Heisenberg behavior (Eq. 10). The calculated J values (in cm^{-1}) obtained are collected in Table 5, together with the experimental ones. The dominant interaction is the nearest neighbor coupling, J_{12}, as expected, with J_{23} being almost negligible for all the compounds. The comparison of the experimental and DDCI values indicates that DDCI(3/3) reproduces correctly the spin-state/energy profiles, while the splitting shows only a qualitative agreement, the theoretical estimates being only about 55-60% of the experimental value. This is not an isolate case. In fact, while DDCI approach on a minimal active space has been successful in the evaluation of J on antiferromagnetic compounds, the same performance has not been observed for ferromagnetic compounds. And this is not a difficulty pertinent solely to DDCI. In fact, recent DFT calculations on hetero triply-bridged dinuclear Cu(II) compounds found similar difficulties to reproduce the ferromagnetic coupling.7 The results reproduce qualitatively the experimental behavior but not the fine details along the series of compound explored.

Table 6. Calculated vs fitted magnetic coupling constants (cm^{-1}) in complexes **1-4.** For compound **4**, J_{13} in parentheses, for the rest, J_{12}=J_{13}.

	DDCI(3/3)		DDCI2(7/5)		Fitted	
Complex	J_{12}	J_{23}	J_{12}	J_{23}	J_{12}	J_{23}
1	40.8	0.2	69.3	2.1	76.8	0.5
2	35.6	0.3	77.1	2.8	65.2	-7.0
3	34.4	2.2	72.8	2.7	58.4	-6.9
4	28.9 (1.8)	-0.4			51	-5
AWEQEZ	37.8	0.3	71.6	-1.3	66	**--**

However, when the active space is extended including the bridging ligand orbitals which play a crucial role in the ferromagnetic coupling (here two occupied orbitals centered on the O bridging ligands), the agreement is remarkably improved, even when staying at the DDCI2 level (in this case, only the double excitations involving two active orbitals are considered). A detailed analysis of the key role of these bridging orbitals is out of the scope of this work, and will be discussed elsewhere.**Errore. Il segnalibro non è definito.** The improvement brought by such an approach is clearly shown in the results reported in Table 6 for the four compounds studied here and for compound AWEQEZ which is isostructural with **1** and shows similar trends that those observed for compounds **1-3**.

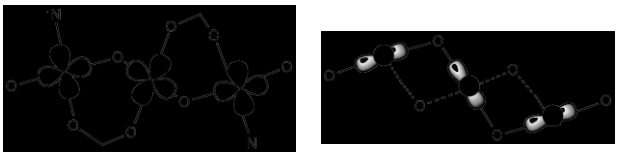

Scheme 2. Two views of the relative orientation of the active Cu 3d orbitals in compounds **1-3**.

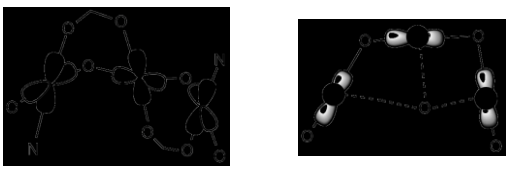

Scheme 3. Two views of the relative orientation of the active Cu 3d orbitals in compound **4**.

The dominant interaction between the terminal and central Cu sites J_{12} is quantitatively reproduced, showing in all cases a coupling ferromagnetic in nature. This behavior is in agreement with that found in mixed bridged binuclear Cu(II) compounds where Cu centers are bridged by alkoxide and carboxylate ligands. These two groups are countercomplementary following the concept introduced by Nishida et al.[15] and McKee et al.[16] in the sense that one of the ligand orbitals has the correct symmetry to mix with the combination of the Cu 3d orbitals to form an antibonding M-L orbital, while the other has not net overlap (scheme 4). As a result of this countercomplementarity, a ferromagnetic interaction between the metal centers is expected. The same concept has also been invoked previously to explain the magnetic behaviour of mixed μ-acetato μ-hydroxo dinuclear and trinuclear Cu(II) complexes.[10d,13] Our calculations, however, indicate that these two ligands contribute differently to the Cu-Cu magnetic coupling. In fact, the carboxylate group is just a spectator in the coupling, by completing the coordination sphere of Cu and impossing a certain geometry and orientation of the two centers, while the alkoxide ligand is crucial for the coupling as demonstrated by the fact that the calculated *J* values agree with the experimental ones when just the two orbitals of the alkoxide ligands are included in the active space.

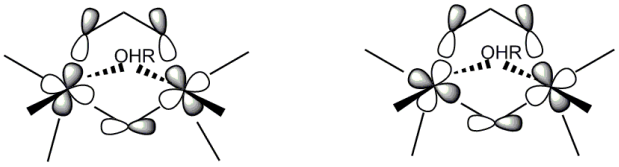

Scheme 4. Overlap between Cu 3d orbitals and alkoxide and carboxylate orbitals.

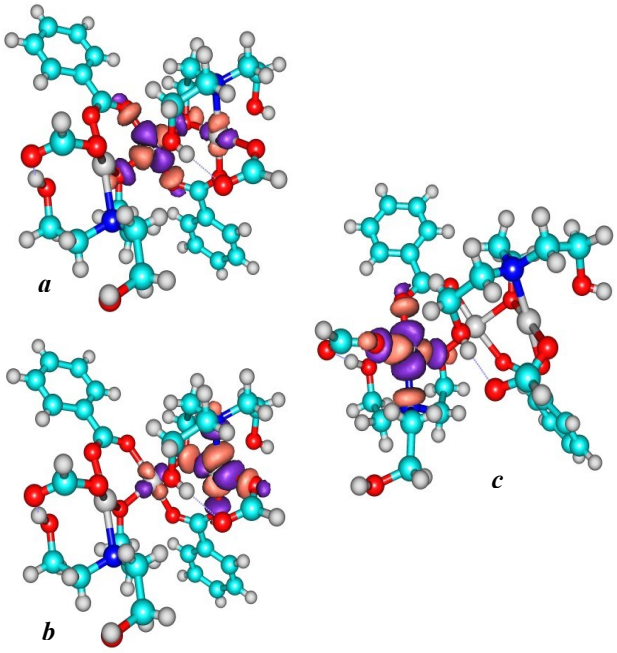

Figure 19. Quartet state active orbitals of complex **4** obtained from a CASSCF(3/3) calculation. "a" and "b" correspond to the symmetric and antisymmetric combination of the Cu1 and Cu2 3d orbitals, with small tails on ligands, while "c" is essentially localized on the terminal Cu3 atom.

In the case of compound 4, the situation is different as expected from the particularities of its structure. Three different J values can be distinguished. At DDCI(3/3) level, the dominant interaction is ferromagnetic in nature, between central Cu1 and terminal Cu2 ions, with a value J_{12}=28.9 cm^{-1} close to that found for the other systems. In contrast, the interaction between Cu1 and Cu3 is ferromagnetic but one order of magnitude smaller (J_{13}=1.8 cm^{-1}). Finally, the interaction between the terminal centers is negligible (J_{23} = -0.4 cm^{-1}). Although the evaluation of the coupling constants in this system at DDCI2(7/5) level faces some technical problems, it is reasonable to expect a similar trend that those observed for the other systems at this level, i.e. an enhancement of the ferromagnetic contribution in the dominant interaction, that finally controls the macroscopic behavior of the system.

On the other hand, the X-ray data confirm the presence of intermolecular hydrogen bonds. This type of intermolecular contacts has been shown to play a crucial role in the magnetic properties of dinuclear copper complexes in the past.[51] To check their potential impact on the magnetic behavior, we have also evaluated the amplitude of the coupling between terminal Cu atoms on

two neighboring trimer molecules of complex **1**. The model employed is shown in Fig. 20, together with the relative orientation of the two active orbitals. The system contains only two unpaired electrons on two magnetic orbitals, and the intramolecular magnetic coupling J_{inter} can be evaluated from the singlet-triplet energy difference. The DDCI value for this interaction indicates that the coupling is negligible, $J_{inter} \sim 0.1$ cm^{-1}. This result validates the spin model employed in the fitting based on isolated trimer units.

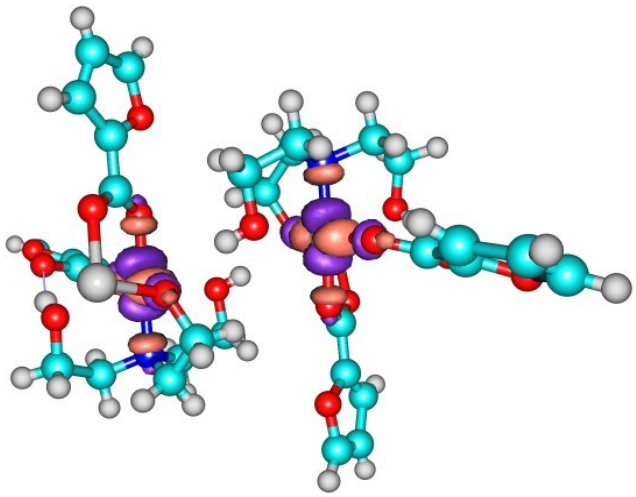

Figure 20. Relative orientation of the Cu 3d magnetic orbitals on intermolecular interactions in complex **1**.

Conclusions

We have synthesized four new trinuclear Cu(II) complexes with formula $[Cu_3(R\text{-}COO)_4(H_2TEA)_2]$, where $RCOO^-$ is 2-furoate (**1**), 2-methoxybenzoate (**2**) and 3-methoxybenzoate (**3**, **4**). The crystal structures were solved and the magnetic properties studied by magnetic susceptibility measurements as a function of temperature. The **1-3** complexes present similar features, resulting from very close coordination geometries around the three Cu atoms. Complex **4** (polymorph of **3**) is different as far as both the overall conformation and central Cu coordination geometry are concerned. Here, the protonated oxygen of the H_2TEA ligand is bound to all the three copper atoms, bringing the lateral Cu nearer to each other. High-field EPR spectroscopy allowed to determine accurately the zero-field splitting parameters, including their sign, for both the dimeric and trinuclear complexes **1-3** and AWEQEZ[12a] which

particularly in the case of the trinuclear systems seems to be a major step forward compared to past research.

The magnetic studies yielded J_{12} values of 76.8, 65.2, 58.4 and 51 cm^{-1} for **1-4**, respectively, showing that the dominant interaction between the terminal and central Cu sites J_{12} is ferromagnetic in nature in all complexes, while the interaction between the terminal centers J_{23} is negligible. A closer inspection to this last interaction shows a disagreement between the fitted and calculated J_{23} values for compounds **2-3**. Our calculations provide a very weak and ferromagnetic interaction, in agreement with the relative orientation and distance between the two terminal Cu $3d_{x^2-y^2}$ orbitals, while the fitted χ-vs-T curve only has an acceptable agreement factor when J_{23} is forced to be antiferromagnetic. Since this interaction is not the leading one this discrepancy does not have a crucial impact on the macroscopic behavior of these complexes, but it puts in evidence the difficulties and limitations of both the experimental fitting and the theoretical calculations when dealing with these large and complex systems.

Supplementary information

Geometric parameters for compounds **1-4**, hydrogen bonding parameters for compounds **1-4,** EPR spectra of $[Cu_2(2\text{-furoate})_2(H_2TEA)_2]$, $[Cu_3(2\text{-ThiophenylCOO})_4(H_2TEA)_2]$, $[Cu_2(p\text{-}OCH_3COO)_2(H_2TEA)_2](H_2O)_2$ and of the dimeric "paddlewheel" intermediates, frequency dependencies of prominent EPR resonances for **4**, reflectance UV-VIS spectra, checkcif reports for **1-4.** Crystallographic data for the structural analysis of compounds **1-4** have been deposited at the Cambridge Crystallographic Data Center, 12 Union Road, Cambridge, CB2 1EZ, UK, and are available free of charge from the Director on request quoting the deposition number CCDC 1004692, 1402372, 1402373 and 1402374 for **1-4**, respectively

Acknowledgments

RPS thanks the University Grants Commission, New Delhi(India) for financial support. The high-field EPR spectra were recorded at the NHMFL which is supported by the NSF through the cooperative agreement DMR-1157490, the State of Florida and the Department of Energy. JJ is grateful to the Ministry of Science and Higher Education of the Polish Republic for financial support in her statutory activities of the Faculty of Chemistry of Wroclaw University. CJC

acknowledges the financial support of the Universidad de Sevilla (Spain) and the technical support of the Supercomputing Team of the Centro Informático Científico de Andalucia (CICA). We thank Dr. A. Wojciechowska (Chemistry Department, Wroclaw University of Technology) for running the UV-VIS spectra. CA, VF and FS would like to acknowledge the support of the University of Ferrara that sponsored the Internationalization Project MolMagRes.

For Table of Contents Only

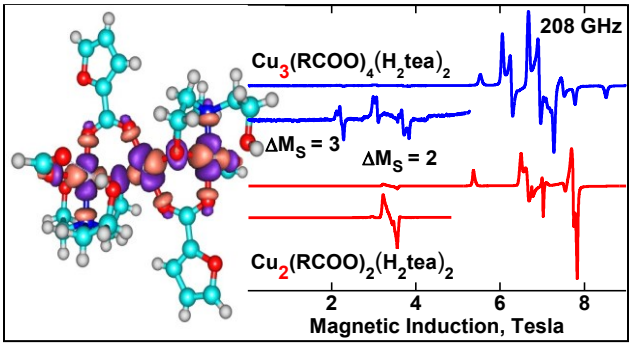

Four new trinuclear $[Cu_3(R\text{-}COO)_4(H_2TEA)_2]$ copper(II) complexes were prepared and characterized by a multifaceted approach including magnetic susceptibility measurements, high-field EPR, single crystal X-ray structure determination and DDCI calculations. The trinuclear systems exhibit a dominant ferromagnetic interaction between the central and terminal Cu atoms, and considerable variation in the zero-field splitting parameters (zfs). Three dimeric complexes, closely related to the trinuclear compounds, were also investigated.

References

(1) Bogani, L; Wernsdorfer W. *Nature Mater.* **2008,** *7*, 179-186.

(2) (a) *Copper Coordination Chemistry: Biochemical and Inorganic Perspectives;* Karlin, K.D.; Zubieta, J., Eds.; Adenine Press, New York, 1983. (b) Thompson L. K. *Coord. Chem. Rev.* **2002**, *193,* 233-234. (c) Ruben, M.; Rojo, J.; Romero-Salguero, F.J.; Uppadine, L.H.; Lehn, J.-M. *Angew. Chem. Int. Ed.* **2004**, *43*, 3644-3662. (d) Ruben, M.; Lehn, J.-M.; Muller, P. *Chem. Soc. Rev*. **2006**, *35*, 1056-1067. (e) Plass, W. *Coord. Chem. Rev*. **2009**, *253*, 2286-2295. (f) Hatfield, W.E. in *Magnetostructural Correlations in Exchange Coupled Systems*; Willet, R.D.; Gatteschi, D.; Kahn, O., Eds.; Reidel, Dordrech, The Netherlands, 1985. (g) Sletten, J.; Sorensen, A.; Julve, M.; Journaux, Y. *Inorg. Chem*. **1990**, *29*, 5054-5058. (h) Murray, K.S. *Adv. Inorg. Chem*. **1995**, *43*, 261-358.

(3) Kirillov, A.M.; Kirillova, M.V.; Pombeiro, A.J.L. *Coord. Chem. Rev*. **2012**, *256*, 2741-2759.

(4) Zhao, Y.; Zhu, J.; He , W.; Yang, Z.; Zhu, Y.; Li, Y.; Zhang, J.; Guo, Z. *Chem. Eur. J*. **2006**, *12*, 6621-6629.

(5) (a) Solomon, E. I.; Sundaram, U. M.; Machonkin, T. E. *Chem. Rev*. **1996,** *96*, 2563-2605. (b) Solomon, E. I.; Chen, P.; Metz, M.; Lee, S.-K.; Palmer, A.E. *Angew. Chem. Int. Ed*. **2001**, *40*, 4570-4590. (c) Kitajima, N.; Moro-Oka, Y. *Chem. Rev*. **1994**, *94*, 737-757. (d) Chen, P.; Solomon, E. I. *PNAS* **2004**, *101*, 13105-13010. (e) Chufán, E. E.; Puiu, S. C.; Karlin, K. D. *Acc. Chem. Res*. **2007**, *40*, 563-572. (f) Solomon, E. I.; Sarangi , R.; Woertink , J. S.; Augustine, A. J.; Yoon, J.; Ghosh, S. *Acc. Chem. Res.* **2007**, *40*, 581-591.

(6) Tegoni, M.; Remelli, M. *Coord. Chem. Rev*. **2012**, *256*, 289-315.

(7) (a) Wannarit, N.; Siriwong, K.; Chaichit, N.; Youngme, S.; Costa, R.; Moreira, I. de P. R.; Illas, F. *Inorg. Chem*. **2011**, *50*, 10648-10659. (b) Costa, R.; Moreira, I. de P.R.; Youngme, S.; Siriwong, K.; Wannarit, N.; Illas, F. *Inorg. Chem*. **2010**, *49*, 285-294. (c) Wannarit, N.; Pakawatchai, C.; Mutikainen, I.; Costa, R.; Moreira, I. de P. R.; Youngme S.; Illas, F. *Phys. Chem. Chem. Phys.* **2013**, *15*, 1966-1975. (d) Youngme, S.; Phatchimkun, J.; Chaichit, N.; Meejoo, S.; van Albada, G.A.; Reedijk, J. *Polyhedron* **2008**, *27,* 304-318.

(8) Sharma, R. P.; Saini, A.; Venugopalan, P.; Ferretti, V.; Spizzo, F.; Angeli, C.; Calzado, C. J. *New J. Chem.* **2014**, *38*, 574-583.

(9) (a) Saini, A.; Sharma, R.P.; Kumar, S.; Venugopalan, P.; Gubanov, A.I.; Smolentsev, A.I. *Polyhedron* **2015,** *100*, 155–163. (b) Saini, A.; Sharma, R.P.; Kumar, S.; Venugopalan, P.; Starynowicz, P.; Jezierska, J. *Inorg. Chim. Acta* **2015**, *436*, 169–178. (c) Kumar, S.; Sharma, R.P.; Venugopalan, P.; Jezierska, J.; Wojciechowska, A.; Ferretti, V. *Inorg. Chim. Acta* **2015**, *432,* 221-230. (d) Kumar, S.; Sharma, R.P.; Venugoapalan, P.; Aree, T.; Ferretti,V. *J. Mol. Struct.* **2015**, *1092*, 225-232. (d) Kumar, S.; Sharma, R.P.; Saini, A.; Venugoapalan, P.; Ferretti, V. *J. Mol. Struct.* **2015**, *1083*, 398-404. (e) Sharma, R.P.; Kumar, S.; Saini, A.; Venugopalan, P.; Rodríguez-Diéguez, A.; Salas, J.M. *J. Mol. Stuct.* **2014**, *1071*, 11-17. (f) Sharma, R.P.; Saini, A.; Kumar, S.; Venugopalan, P.; Ferretti, V. *J. Mol. Struct.* **2014**, *1067*, 210-215**.** (g) Sharma, R.P.; Saini, A.; Kumar, S.; Venugopalan, P.; Ferretti, V. *J. Mol. Struct.* **2014**, *1060*, 256-263.

(10) (a) Fleischhauer, P.; Gehring, S.; Saal, C.; Haase, W.; Tomkowicz, Z.; Zanchini, C.; Gatteschi, D.; Davidov, D.; Barra, A. L. *J. Magn. Magn. Mater***. 1996**, *159*, 166-174. (b)

Tomkowicz, Z.; Haase, W.; Fleischhauer, P.; Krupski, H.; Micklitz, H.; Friedt, O.; Ściesińska, E.; Ściesiński, J.; Sczaniecki, P. *J. Magn. Magn. Mater.* **2001**, *236*, 347-356. (c) Van Slageren, J.; Ahmedova, A.; Gatteschi, D.; Massa, C. A.; Pardi, L. A. *Inorg. Chim. Acta* **2003**, *351*, 59-62. (d) Gutierrez, L.; Alzuet, G.; Real, J. A.; Cano, J; Borras, J; Castiñeiras, A. *Inorg. Chem.* **2000**, *39,* 3608-3614. (e) Tomkowicz, Z,; Fleischhauer, P.; Haase, W.; Baran, M.; Szymczak, R.; Zaleski, A. J.; Jablonski, R. *J. Magn. Magn. Mater*. **1997**, *172*, 128-138. (f) Gehring, S.; Fleischhauer, P.; Paulus, H.; Haase, W. *Inorg. Chem*. **1993**, *32*, 54-60.

(11) Tudor, V.; Kravtsov, V.Ch.; Julve, M.; Lloret, F.; Simonov, Y. A.; Averkiev, B. B.; Andruh, M. *Inorg. Chim. Acta* **2005**, *358* , 2066-2072.

(12) (a) Boulsourani, Z.; Tangoulis, V.; Raptopoulou, C. P.; Psycharis, V.; Dendrinou-Samara, C. *Dalton Trans.* **2011**, *40*, 7946-7956. (b) Panagoulis, D.; Pontiki, E. Skeva, E.; Raptopoulou, C.; Girousi S. D.; Hadjipavlou-Litina, C.; Dendrinou-Samara, C. *J. Inorg. Biochem*. **2007,** *101*, 623-634.

(13) Escovar, R.M.; Thurston, J.H.; Ould-Ely, T.; Kumar, A.; Whitmire, K.H. *Z. Anorg. Allg. Chem.* **2005**, *631*, 2867-2876.

(14) (a) Ruiz, E.; Alemany, P.; Alvarez, S.; Cano, J. *J. Am. Chem. Soc.* **1997**, *119*, 1297-1303. (b) Ruiz, E.; Alemany, P.; Alvarez, S.; Cano, J. *Inorg. Chem.* **1997**, *36*, 3683-2688. (c) Doyle, R. P.; Julve, M.; Lloret, F.; Nieuwenhuyzen, M.; Kruger, P. *Dalton Trans.* **2006**, 2081-2088.

(15) a) Nishida, Y.; Kida, S. *J. Chem. Soc. Dalton Trans*. *1986*, 2633-2640. b) Nishida, Y.; Takeuchi, M.; Takahashi, K.; Kida, S. *Chem. Lett.* **1985**, 631-634; c) Nishida, Y.; Takeuchi, M.; Takahashi, K.; Kida, S. *Chem. Lett*. **1983**, 1815-1818.

(16) McKee, V.; Zvagulis, M.; Reed, C. A. *Inorg. Chem*. **1985**, *24,* 2914-2919.

(17) Malati, M. A. *Experimental Inorganic Chemistry*, 1st Ed, Harwood Publishing, Chichester, 1999.

(18) Blessing, R. H. *Acta Crystallogr*. **1995**, *A51,* 33-38.

(19) Altomare, A.; Burla M.C.; Camalli, M.; Cascarano, G.; Giacovazzo, C.; Guagliardi, A.; Moliterni, A.G.; Polidori, G.; Spagna, R. *J. Appl. Crystallogr*. **1999**, *32*, 115-119.

(20) Sheldrick, G. M. *SHELXL97, Program for Crystal Structure Refinement*, University of Göttingen, Göttingen, Germany, 1997.

(21) Farrugia, L.J. *J. Appl. Crystallogr*. **1999**, *32*, 837-838.

(22) (a) O'Connor, C. J. *Prog. Inorg. Chem*. **1982**, *29*, 203-283. (b) Bain, G. A.; Berry, J. F. *J. Chem. Ed.* **2008**, *85*, 532-536.

(23) Hassan, A. K.; Pardi, L. A.; Krzystek, J.; Sienkiewicz, A.; Goy, P.; Rohrer, M.; Brunel, L.-C. *J. Magn. Reson.* **2000**, *142*, 300-312.

(24) Burnett, M.N.; Johnson, C.K. ORTEPIII. *Oak Ridge Thermal Ellipsoid Plot Program for Crystal Structure Illustrations*, Report ORNL-6895, Oak Ridge National Laboratory, Oak Ridge, Tennessee, USA, 1996.

(25) (a) Bellamy, L.J. *The Infrared Spectra of Complex Molecules*, 2nd Ed. Vol. 2, Chapman & Hall, London/New York, 1980. (b) Nakamoto, K. *Infrared and Raman Spectra of Inorganic and Coordination Compounds*, 5th Ed., John Wiley & Sons, New York , 1997.

(26) (a) Das, M.; Shivashankar, S.A. *Applied Organomet. Chem*. **2007**, *21*, 15-25. (b) Topcu, Y.; Andac, O.; Yilmaz, V.T.; Harisson, W. *J. Coord. Chem*. **2002**, *55*, 805-815.

(27) Bencini, A.; Gatteschi, D. *EPR of Exchange Coupled Systems.* Springer Verlag, Berlin, 1990.

(28) Sharma, R.P.; Saini, A.; Monga, D.; Venugopalan, P.; Jezierska, J.; Ozarowski, A.; Ferretti, V. *New J. Chem.* ***2014****, 38*, 437-447.

(29) (a) Ozarowski, A. *Inorg. Chem*. **2008**, *47*, 9760-9762. (b) Ozarowski, A.; Szymanska, I. B.; Muziol, T.; Jezierska, J. *J. Am. Chem. Soc*. **2009**, *131*, 10279-10292. (c) Semenaka, V. V.; Nesterova, O. V.; Kokozay, V. N.; Dyakonenko, V. V.; Zubatyuk, R. I.; Shishkin, O. V.; Boca, R.; Jezierska, J.; Ozarowski, A. *Inorg. Chem.* **2010**, *49*, 5460-5471.

(30) (a) Senchyk, G.A.; Lysenko, A.B.; Rusanov, E.B.; Chernega, A.N.; Jezierska, J.; Domasevitch, K.V.; Ozarowski, A. *Eur. J. Inorg. Chem*. **2012**, *35*, 5802-5813. (b) Aznar, E.; Ferrer, S.; Borras, J.; Lloret, F.; Liu-Gonzalez, M.; H. Rodriguez-Prieto, H.; Garcia-Granda, S. *Eur. J. Inorg. Chem*. **2006**, *24*, 5115-5125.

(31) (a) Moriya, T. *Phys. Rev.* **1960**, *120*, 91-98. (b) Yoon, J.; Solomon, E. I. *Coord. Chem. Rev.* **2007**, *251*, 379-400. (c) Ferrer, S.; Lloret, F.; Pardo, E.; Clemente-Juan, J. M.; Liu- González, M.; García-Granda, S. *Inorg. Chem.* **2012**, *51*, 985-1001. (d) Vasylevskyy, S. I.; Senchyk, G. A.; Lysenko, A. B.; Rusanov, E. B.; Chernega, A. N.; Jezierska, J.; Krautscheid, A.; Domasevitch, K. V. Ozarowski, A. *Inorg. Chem.* **2014**, *53,* 3642-3654. (e) Boča, R.; Herchel, R. *Coord. Chem. Rev*. **2010**, *254*, 2973-3025.

(32) (a) Maurice, R.; Sivalingam, K.; Ganyushin, D.; Guihery, N.; de Graaf, C.; Neese, F. *Inorg. Chem.* **2011,** *50*, 6229-6236. (b) Gribnau, M. C. M.; Keijzers, C. P. *Inorg. Chem.* **1987**, *26*, 3413-3414. (c) Ross, P. K.; Allendorf, M. D.; Solomon, E. I. *J. Am. Chem. Soc.* **1989**, *111*, 4009-4021. (d) Singh, S. K.; Rajaraman, G. Chem. Eur. J. **2014**, *20*, 5214-5218. (f) Atanasov, M.; Comba, P.; Hanson, G. R.; Hausberg, S.; Helmle, S.; Wadepohl, H. *Inorg. Chem.* **2011**, *50*, 6890-6901.

(33) Note that if the Z axis were chosen along the Cu-Cu direction, the formulas would be different: $D_{dip} = -(4g_x^2 + g_y^2 + g_z^2)\mu_B^2/4R^3_{Cu\text{-}Cu}$, $E_{dip} = (g_z^2 - g_y^2)\mu_B^2/4R^3_{Cu\text{-}Cu}$

(34) Riplinger, C.; Kao, J. P.Y.; Rosen, G. M.; Kathirvelu, V.; Eaton, S. S.; Kutateladze, A.; Neese, F. *J. Am. Chem. Soc*. **2009**, *131*, 10092-10106.

(35) (a) Reger, D.L.; Pascui, A.E.; Smith, M.D.; Jezierska, J.; Ozarowski, A. *Inorg. Chem*. **2015**, *54*, 1487-1500. (b) Reger, D.L.; Pascui, A.E.; Foley, E.A.; Smith, M.D.; Jezierska, J.; Ozarowski, A. *Inorg. Chem*. **2014**, *53*, 1975-1988. (c) Reger, D.L.; Pascui, A.E.; Smith, M.D.; Jezierska, J.; Ozarowski, A. *Inorg. Chem*. **2012**, *51*, 11820-11836. (d) Reger, D.L.; Pascui, A.E.; Smith, M.D.; Jezierska, J.; Ozarowski, A. *Inorg. Chem*. **2012**, *51*, 7966-7968.

(36) (a) Calzado, C. J.; Malrieu, J.P. *Phys. Rev. B* **2001,** *63*, 214520. (b) Calzado, C. J.; Malrieu, J.P. *Eur. Phys. J. B* **2001,** *21***,** 375-381. (c) Calzado, C. J.; Malrieu, J.P. *Phys. Rev. B* **2004**, *69*, 0944351. (d) Calzado, C. J.; de Graaf, C.; Bordas, E.; Caballol, R.; Malrieu, J. P. *Phys. Rev. B*

2003, *67*, 132409. (e) Malrieu, J.P.; Caballol,R.; Calzado, C.J.; de Graaf, C.; Guihery, N. *Chem.Rev.* **2014**, *114*, 429-492.

(37) (a) Miralles, J.; Daudey, J. P.; Caballol, R. *Chem. Phys. Lett*. **1992**, *198*, 555-562; (b) Miralles, J.; Castell, O.; Caballol, R.; Malrieu, J. P. *Chem. Phys*. **1993**, *172,* 33-43.

(38) (a) Oms, O.; Rota, J. B.; Norel, L.; Calzado, C. J.; Rousseliere, H.; Train C.; Robert, V. *Eur. J. Inorg. Chem*. **2010**, 5373-5378. (b) Bandeira, N. A. G.; Maynau, D.; Robert, V.; Le Guennic, B. *Inorg. Chem*. **2013**, *52*, 7980-7986. (c) Vérot, M.; Rota, J. B.; Kepenekian, K.; Le Guennic B.; Robert, V. *Phys. Chem. Chem. Phys*. **2011**, *13*, 6657-6661; (d) Aronica, C.; Chastanet, G.; Pilet, G.; Le Guennic, B.; Robert, V.; Wernsdorfer, W.; Luneau, D. *Inorg. Chem*. **2007**, *46*, 6108-6119.

(39) (a) Calzado, C. J.; Sanz, J.F.; Malrieu, J.P. *J. Chem. Phys.* **2000**, *112*, 5158-5167. (b) Calzado, C. J.; Evangelisti, S.; Maynau, D. *J. Phys. Chem. A*, **2003**, *107*, 7581-7588.

(40) (a) Casanovas, J.; Illas, F. *J. Chem. Phys.* **1994**, *100*, 8257-8264. (b) Moreira, I. de P. R.; Illas, F.; Calzado, C. J.; Sanz, J.; Malrieu, J. P.; Ben Amor, N.; Maynau, D. *Phys. Rev. B*, **1999**, *59*, 6593-6596. (c) de Graaf, C.; Moreira, I. de P. R.; Illas, F.; Martin, R.L. *Phys. Rev. B*, **1999**, *60*, 3457-3464. (d) Muñoz, D.; Illas, F.; Moreira, I. de P. R. *Phys. Rev. Lett*. **2000**, *84*, 1579-1582.

(41) (a) Cabrero, J.; de Graaf, C.; Bordas, E.; Caballol, R.; Malrieu, J.P. *Chem. Eur. J*. **2003**, *9*, 2307-2315. (b) Queralt, N.; Taratiel, D.; de Graaf, C.; Caballol, R.; Cimiraglia, R.; Angeli, C. *J. Comput. Chem*. **2008**, *29*, 994-1003.

(42) Suaud, N.; Gaita-Arino, A.; Clemente-Juan, J. M.; Sanchez-Marin, J.; Coronado, E. *J. Am. Chem. Soc.* **2002**, *124*, 15134-15140.

(43) (a) Barone, V.; Cacelli, I.; Ferretti, A.; Monti, S.;Prampolini, G. *J. Chem. Theory Comput*. **2011**, *7*, 699-706. (b) Barone, V.; Cacelli, I.; Ferretti,A.; Monti, S.; Prampolini, G. *Phys. Chem. Chem. Phys.* **2011**, *13*, 4709-4714.

(44) (a) Neese, F. *J. Am. Chem. Soc*. **2006**, *128*, 10213-10222. (b) Liakos, D. G.; Ganyushin, D.; Neese, F. *Inorg. Chem.* **2009**, *48*, 10572-10580. (c) Ganyushin, D.; Gilka, N.; Taylor, P. R.; Marian, C. M.; Neese, F. *J. Chem. Phys*. **2010**, *132*, 144111. (d) McNaughton, R. L.; Roemelt, M.; Chin, J. M.; Schrock, R. R.; Neese, F.; Hoffman, B.M. *J. Am. Chem. Soc*. **2010**, *132*, 8645-8656.

(45) (a) Miralles, J.; Caballol, R.; Malrieu, J.-P. *Chem. Phys*. **1991**, *153*, 25-37. (b) Calzado, C. J.; Malrieu, J.-P.; Cabrero, J.; Caballol, R. *J. Phys. Chem. A* **2000**, *104*, 11636-11643.

(46) (a) Calzado, C. J. ; Evangelisti, S. *Dalton Trans*. **2014**, *43*, 2988-2996. (b) Rota, J.B. ; Calzado, C. J. ; Train, C. ; Robert, V. *J. Chem. Phys*. **2010**, *132*, 154702. (c) Rota, J. B.; Norel, L.; Train, C.; Ben Amor, N.; Maynau, D. ; Robert, V. *J. Am. Chem. Soc*. **2008**, *130*, 10380-10385; (d) Castell, O.; Caballol, R.; García, V.M.; Handrick, K. *Inorg. Chem*. **1996**, *35*, 1609-1615; (e) Calzado, C. J. ; Clemente-Juan, J.M. ; Coronado, E. ; Gaita-Ariño, A. ; Suaud, N. *Inorg. Chem*. **2008**, *47*, 5889-5901.

(47) Barandiarán, Z.; Seijo, L. *Can. J. Chem*. **1992,** *70***,** 409-415.

(48) (a) Widmark, P.-O.; Malmqvist, P.-A.; Roos, B.O. *Theor. Chim. Acta* **1990,** *77*, 291-306. (b) Widmark, P.-O.; Persson, B.J.; Roos, B.O. *Theor. Chim. Acta,* **1991,** *79*, 419-432. (c) Pierloot, K.; Dumez, B.; Widmark, P.-O.; Roos, B.O. *Theor. Chim. Acta* **1995,** *90***,** 87-114.

(49) Aquilante, F.; de Vico, L.; Ferré, N.; Ghigo, G.; Malmqvist, P.-A.; Pedersen, T.; Pitonak, M.; Reiher, M.; Roos, B.O.; Serrano-Andrés, L.; Urban, M.; Veryazov, V.; Lindh, R. *J. Comput. Chem*. **2010,** *31*, 224-247.

(50) CASDI program: Ben Amor, N. ; Maynau, D. *Chem. Phys. Lett.* **1998,** *286*, 211-220, package developed at the Laboratoire de Chimie et Physique Quantiques, Université Paul Sabatier, Toulouse (France).

(51) (a) Sanchez Costa, J.; Bandeira, N. A. G; Le Guennic, B.; Robert, V.; Gamez, P.; Chastanet, G.; Ortiz-Frade, L.; Gasque, L. *Inorg. Chem*. **2011**, *50*, 5696-5705. (b) Moreno, J. M.; Ruiz, J.; Dominguez-Vera, J. M.; Colacio, E. *Inorg. Chim. Acta* **1993**, *208*, 111-115. (c) Plass, W.; Pohlmann, A.; Rautengarten, J. *Angew. Chem., Int. Ed*. **2001**, *40*, 4207-4210. (d) Valigura, D.; Moncol, J.; Korabik, M.; Pucekova, Z.; Lis, T.; Mrozinski, J.; Melnik, M. *Eur. J. Inorg. Chem*. **2006**, 3813-3817. (e) Tang, J. K.; Costa, J. S.; Golobic, A.; Kozlevcar, B.; Robertazzi, A.; Vargiu, A. V.; Gamez, P.; Reedijk, J. *Inorg. Chem*. **2009**, *48*, 5473-5479. (f) Vaskova, Z.; Moncol, J.; Korabik, M.; Valigura, D.; Svorec, J.; Lis, T.; Valko, M.; Melnik, M. *Polyhedron* **2010**, *29*, 154-163. (g) Desplanches, C.; Ruiz, E.; Rodriguez-Fortea, A.; Alvarez, S. *J. Am. Chem. Soc.* **2002**, *124*, 5197-5205.(h) Le Guennic, B.; Ben Amor, N.; Maynau, D.; Robert, V. *J. Chem. Theory Comput*. **2009,** *5*, 1506-1510.